Inorganic Chemistry

pubs.acs.org/IC

Article

# Mono- and Bis(iminoxolene)iridium Complexes: Synthesis and Covalency in $\pi$ Bonding

Thomas H. Do and Seth N. Brown*

Cite This: *Inorg. Chem.* 2022, 61, 5547−5562

Read Online

ACCESS | Metrics & More | Article Recommendations | Supporting Information

**ABSTRACT:** *N*-(2,6-Diisopropylphenyl)-4,6-di-*tert*-butyl-*o*-iminobenzoquinone (Diso) reacts with the (cyclooctadiene)iridium chloride dimer to form a monoiminoxolene complex, (Diso)Ir(cod)Cl. Reaction of 2 equiv of the iminoquinone with chlorobis(cyclooctene)iridium dimer affords the bis-iminoxolene $(Diso)_2IrCl$. This five-coordinate complex adopts a distorted square pyramidal structure with an apical chloride ligand and undergoes halide exchange to form an air-stable iodide complex. $(Diso)_2IrCl$ can be reduced by one electron to form neutral, square planar $(Diso)_2Ir$, while oxidation with $PhICl_2$ gives octahedral *trans*-$(Diso)_2IrCl_2$. The *cis* isomer can be prepared by air oxidation of $(Diso)_2IrCl$; *cis*/*trans* isomerization is not observed even on prolonged heating. Structural and spectroscopic features of the complexes are consistent with the presence of strong, covalent $\pi$ bonding between the metal and the iminoxolene ligands, with structural data suggesting between 45 and 60% iridium character in the $\pi$ bonding orbitals, depending on the ancillary ligands. The spectroscopic similarity of $(Diso)_2Ir$ and $(Diso)_2IrCl$ to their cobalt congeners suggests that the first-row metal complexes likewise have appreciably covalent metal-iminoxolene $\pi$ bonds.

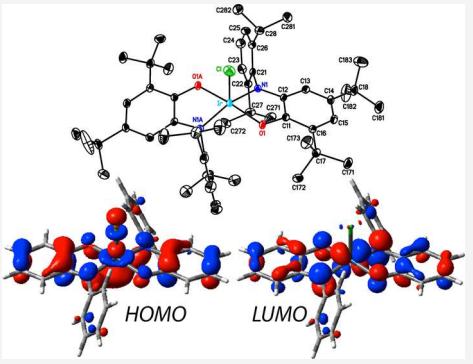




## INTRODUCTION

Iminoxolenes[1] and dioxolenes[2] are quintessential examples of redox-active ligands, capable of adopting various oxidation states from the fully reduced amidophenoxides and catecholates to the fully oxidized iminoquinones and benzoquinones. Their ability to tap into these different oxidation states arises from the redox-active orbital (RAO) of each ligand, an in-phase combination of the heteroatom lone pair orbitals that is $\pi$-antibonding to the filled $\pi$ orbital in the benzene ring (Figure 1).[3] The antibonding interaction puts the RAO at a moderate energy, making a variety of redox states accessible.

Because the iminoxolene RAO is similar in energy to metal d orbitals and of $\pi$ symmetry with respect to the metal, metal-iminoxolene $\pi$ bonding can be quite strong[4] and highly covalent in nature. As one moves from left to right across the periodic table, metal orbitals become lower in energy; early transition metals' d orbitals are thus higher in energy than the iminoxolene RAO, while late transition metals have d orbitals that are lower in energy than the ligand RAO. These mismatches in energy level force the localization of electrons, essentially separating the metal and ligand electronically. Redox changes are thus largely localized on the ligands in complexes of both early transition metals (group 4[5,6] and group 5[7,8]) and late transition metals (group 10[9−11]). However, the transition metals in the middle of the periodic table have d orbitals that are well matched in energy to the ligand RAO. Metals such as molybdenum display a moderate degree of covalency in their bonding, indicated by structural changes in the coordinated iminoxolene that give an oxidation

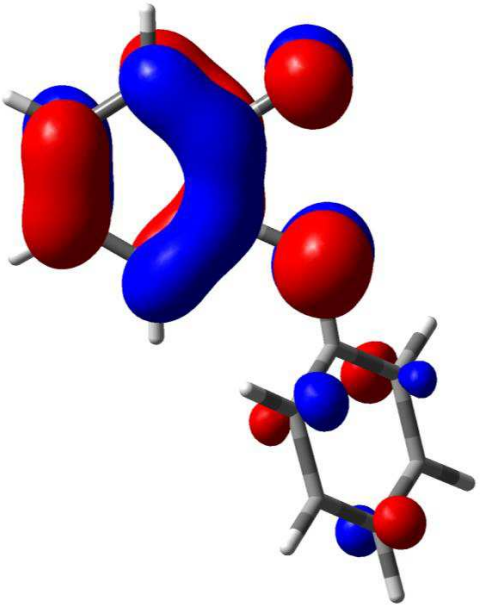

**Figure 1.** RAO of an iminoxolene ligand (LUMO of *N*-phenyl-*o*-iminobenzoquinone).

**Received:** December 27, 2021
**Published:** March 31, 2022





https://doi.org/10.1021/acs.inorgchem.1c04005
*Inorg. Chem.* 2022, 61, 5547−5562

state value between an amidophenoxide and an iminosemiquinone.[12]

Recently, we have shown that the bonding in group 8 metal-iminoxolene complexes is well described by a covalent model with significant electron density in the $\pi$ bonding orbitals on both the ligand and the metal.[13] The distribution of electrons in the bond is affected by the identity of the metal (more metal-centered for Ru, more ligand-centered for Os)[13] and the nature of the ancillary ligands.[14] The bonding of iminoxolenes with the group 9 element iridium thus provides an intriguing test case: Will the iridium-ligand $\pi$ bonding be highly delocalized, similar to osmium and ruthenium, or will it more resemble the more ionic platinum compounds? Known iridium-iminoxolene complexes, all of the form Cp*Ir($OC_6H_2$-2-(NR)-3,5-$^t$Bu$_2$) (R = 2-$CF_3C_6H_4$,[15] $^t$Bu,[16] or 2-$CH_3SC_6H_4$[17]), seem to point to the latter answer, as all have been characterized as iridium(III) amidophenoxides, with one- and two-electron oxidations being largely ligand centered.

Here, we describe the preparation and characterization of new mono- and bis(iminoxolene)iridium complexes containing the ligand derived from *N*-(2,6-diisopropylphenyl)-4,6-di-*tert*-butyl-*o*-iminobenzoquinone (Diso). With this more diverse suite of compounds in hand, it is clear that the behavior of the previously reported pentamethylcyclopentadienyl complexes is atypical; other iridium iminoxolene compounds show evidence of notably covalent $\pi$ bonding.

## RESULTS

**Preparation of Mono- and Bis(iminoxolene) Iridium Monochloride Complexes.** The known Cp*Ir(iminoxolene) complexes are prepared by treatment of the iridium(III) precursor $[Cp^*IrCl_2]_2$ with the appropriate aminophenol in the presence of base.[15−17] Since the iminoquinone *N*-(2,6-diisopropylphenyl)-3,5-di-*tert*-butyl-*o*-iminobenzoquinone (Diso) is readily available,[18] while the preparation of the corresponding aminophenol has not been described,[19] we sought an appropriate iridium(I) reagent to combine with the iminoquinone to arrive at the same final overall oxidation level. The (cyclooctadiene)iridium chloride dimer $[(cod)IrCl]_2$ reacts rapidly with Diso to afford the monoiminoxolene complex (Diso)Ir(cod)Cl in good yield (eq 1). NMR

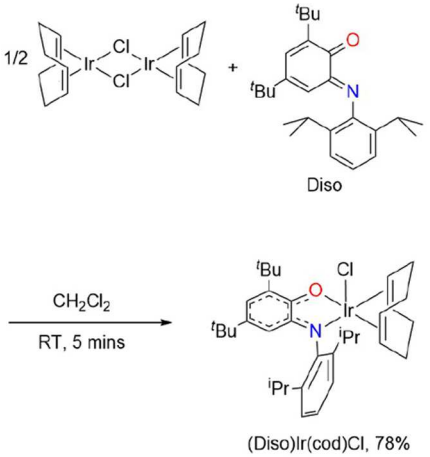


(1)

spectroscopy shows that the compound is completely asymmetric and that both alkenes are coordinated to iridium (as evidenced by the $^{13}$C NMR resonances of the alkene carbons at $\delta$ 71.4, 75.1, 79.7, and 86.1 ppm). This is consistent with the structure in the solid state (Figure 2, Table 1), which is roughly square pyramidal with the chlorine atom apical. The asymmetry of the NMR spectra indicates that pseudorotation of the (cod)Cl fragment relative to the Diso ligand must be slow on the NMR time scale.

Even in the presence of excess Diso, reaction stops at the monoiminoxolene complex. In contrast, reaction of Diso with an iridium(I) starting material that has more labile cyclooctene ligands, $[(coe)_2IrCl]_2$, affords the green bis(iminoxolene) complex $(Diso)_2IrCl$, with no bound cyclooctene (eq 2). (If

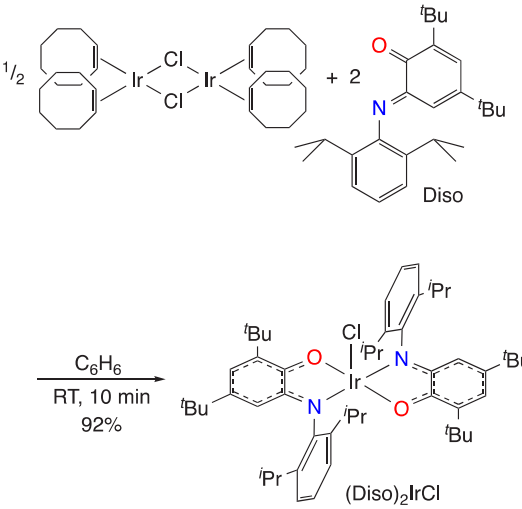


(2)

substoichiometric iminoquinone is used, dimetallic $(Diso)_2Ir(\mu\text{-}Cl)_2Ir(coe)_2$ (Figures S1 and S2, Tables S1 and S2) is observed as a side product.) The bis-iminoxolene compound adopts a roughly square pyramidal geometry ($\tau$[21] = 0.26) with apical chloride (Figure 3). The $^1$H NMR spectrum indicates that the compound is diamagnetic and $C_2$-symmetric, with one methine and one methyl signal appearing unusually upfield ($\delta$ 1.18 and 0.16, respectively, in $CDCl_3$). Halide exchange of $(Diso)_2IrCl$ with NaI leads to clean formation of $(Diso)_2IrI$ (eq 3), which is spectroscopically and structurally (Figure S3,

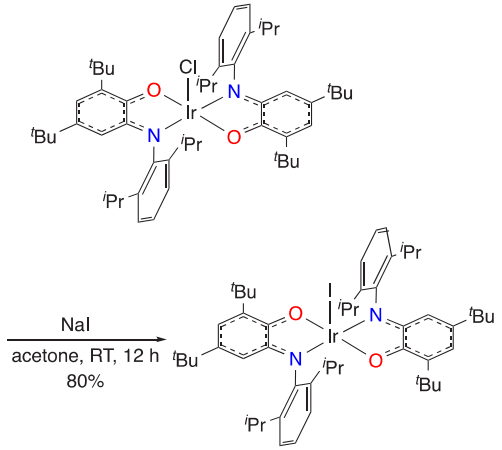


(3)

Table 1) very similar to the chloride complex. In contrast to the air-sensitive chloride, purple $(Diso)_2IrI$ is air and water stable.

**Chlorination and Dechlorination Reactions of $(Diso)_2IrCl$.** Cyclic voltammetry in dichloromethane solution reveals that the monochloride complex $(Diso)_2IrCl$ can undergo both outer-sphere oxidation ($E_{p,a}$ = 0.54 V vs


https://doi.org/10.1021/acs.inorgchem.1c04005
Inorg. Chem. 2022, 61, 5547−5562

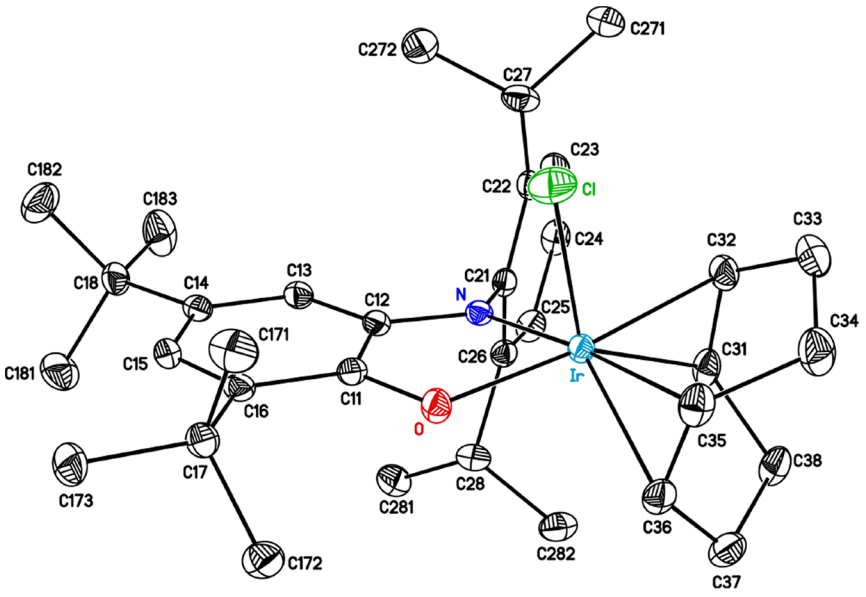


**Figure 2.** Thermal ellipsoid plot of (Diso)Ir(cod)Cl·0.5$CH_3CN$. Hydrogen atoms and lattice solvent molecules have been omitted for clarity. Iridium-alkene distances (Å): Ir−C31, 2.1428(15); Ir−C32, 2.1305(15); Ir−C35, 2.1658(16); Ir−C36, 2.1434(15).

**Table 1. Summary of Crystal Data**

| | (Diso)Ir(cod)Cl·0.5$CH_3CN$ | $(Diso)_2IrCl·3C_6H_6$ | $(Diso)_2IrI·C_3H_6O$ | $(Diso)_2Ir$ | *trans*-$(Diso)_2IrCl_2$ | *cis*-$(Diso)_2IrCl_2$ |
|---|---|---|---|---|---|---|
| molecular formula | $C_{35}H_{50.5}ClIrN_{1.5}O$ | $C_{70}H_{92}ClIrN_2O_2$ | $C_{55}H_{80}IIrN_2O_3$ | $C_{52}H_{74}IrN_2O_2$ | $C_{52}H_{74}Cl_2IrN_2O_2$ | $C_{52}H_{74}Cl_2IrN_2O_2$ |
| formula mass | 735.92 | 1221.10 | 1136.31 | 951.33 | 1022.23 | 1022.23 |
| $T$ (K) | | | 120(2) | | | |
| crystal system | triclinic | orthorhombic | monoclinic | trigonal | monoclinic | monoclinic |
| space group | $P\bar{1}$ | $P2_12_12$ | $P2_1/n$ | $R\bar{3}$ | $P2_1/n$ | $P2_1/n$ |
| $\lambda$ (Å) | | | 0.71073 (Mo K$\alpha$) | | | |
| total data | 56268 | 97546 | 237464 | 72279 | 47530 | 94307 |
| indep refls | 8176 | 9532 | 27124 | 6116 | 5885 | 12469 |
| $R_{int}$ | 0.0224 | 0.0275 | 0.1357 | 0.0544 | 0.0322 | 0.0218 |
| Obsd refls [$I > 2\sigma(I)$] | 7865 | 9139 | 18089 | 5550 | 5186 | 11753 |
| $a$ (Å) | 10.3311(5) | 13.4453(13) | 20.398(2) | 30.709(4) | 11.0507(3) | 18.719(2) |
| $b$ (Å) | 12.2951(5) | 22.813(2) | 21.327(3) | 30.709(4) | 14.3952(4) | 12.0379(13) |
| $c$ (Å) | 13.9453(6) | 10.2898(10) | 26.295(3) | 13.5320(19) | 15.5181(4) | 22.122(2) |
| $\alpha$ (°) | 99.2948(12) | 90 | 90 | 90 | 90 | 90 |
| $\beta$ (°) | 96.8715(13) | 90 | 107.1644(16) | 90 | 106.5966(7) | 92.0584(15) |
| $\gamma$ (°) | 109.1824(12) | 90 | 90 | 120 | 90 | 90 |
| $V$ (Å$^3$) | 1622.45(12) | 3156.1(5) | 10930(2) | 11051(3) | 2365.73(11) | 4981.7(9) |
| $Z$ | 2 | 2 | 8 | 9 | 2 | 4 |
| $\mu$ (mm$^{-1}$) | 4.225 | 2.202 | 3.049 | 2.757 | 2.976 | 2.827 |
| crystal size (mm) | 0.34 × 0.25 × 0.25 | 0.20 × 0.14 × 0.07 | 0.59 × 0.35 × 0.10 | 0.20 × 0.15 × 0.10 | 0.34 × 0.25 × 0.22 | 0.34 × 0.25 × 0.25 |
| refined params | 567 | 470 | 1111 | 407 | 416 | 828 |
| $R1$, $wR2$ [$I > 2\sigma(I)$] | 0.0128, 0.0309 | 0.0157, 0.0376 | 0.0774, 0.1463 | 0.0328, 0.0935 | 0.0188, 0.0359 | 0.0155, 0.0328 |
| $R1$, $wR2$ [all data] | 0.0138, 0.0312 | 0.0172, 0.0380 | 0.1269, 0.1643 | 0.0400, 0.0979 | 0.0242, 0.0378 | 0.0175, 0.0333 |
| goodness of fit | 1.065 | 1.057 | 1.122 | 1.099 | 1.137 | 1.094 |

$Cp_2Fe^+/Cp_2Fe$) and outer-sphere reduction ($E_{p,c}$ = −0.99 V), but neither redox event is reversible (Figure S5). One possible explanation for the lack of reversibility is that reduction is accompanied by dissociation of chloride and that oxidation is accompanied by binding solvent or counterion. Consistent with this, oxidation of $(Diso)_2IrCl$ with iodobenzene dichloride leads to fast formation of air-stable, paramagnetic *trans*-$(Diso)_2IrCl_2$ (eq 4). The $^1H$ NMR of the compound shows paramagnetically broadened and moderately shifted signals (Figure S16), though not all hydrogen environments are observed. The solution magnetic moment of 1.93 $\mu_B$ at room temperature is close to that expected for the spin-only value for a $S = 1/2$ system. The composition of the compound is confirmed by elemental analysis and supported by successful reduction by cobaltocene in THF to reform diamagnetic $(Diso)_2IrCl$. The compound's stereochemistry is confirmed to be *trans* by X-ray crystallography (Figure 4).

While iodobenzene dichloride oxidation of $(Diso)_2IrCl$ produces exclusively the *trans* stereoisomer, *cis*-$(Diso)_2IrCl_2$ can be prepared by air oxidation of $(Diso)_2IrCl$ in a 1:2:2 mixture of benzene:pentane:methanol. The material is isolated in pure form in low (15%) but reproducible yields. The


https://doi.org/10.1021/acs.inorgchem.1c04005
Inorg. Chem. 2022, 61, 5547−5562

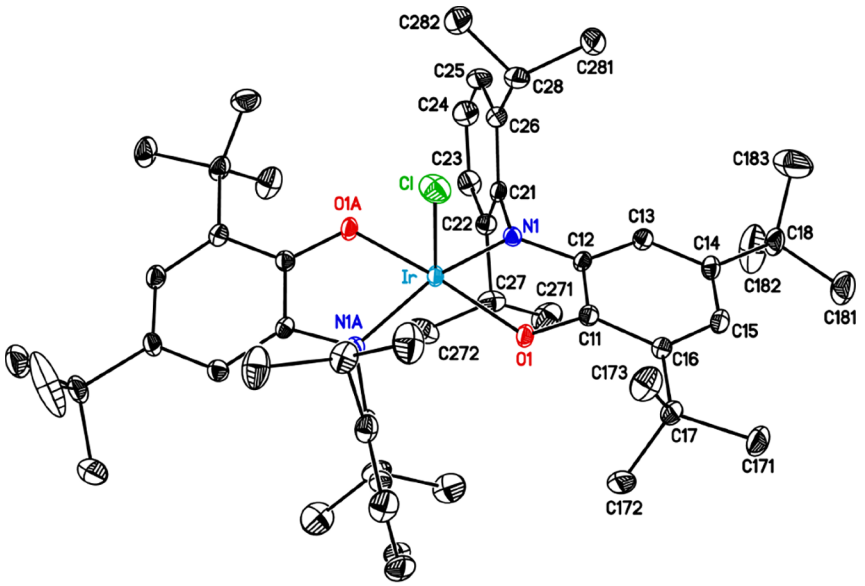


**Figure 3.** Thermal ellipsoid plot of $(Diso)_2IrCl{\cdot}3C_6H_6$. Hydrogen atoms and lattice solvent molecules are omitted for clarity.

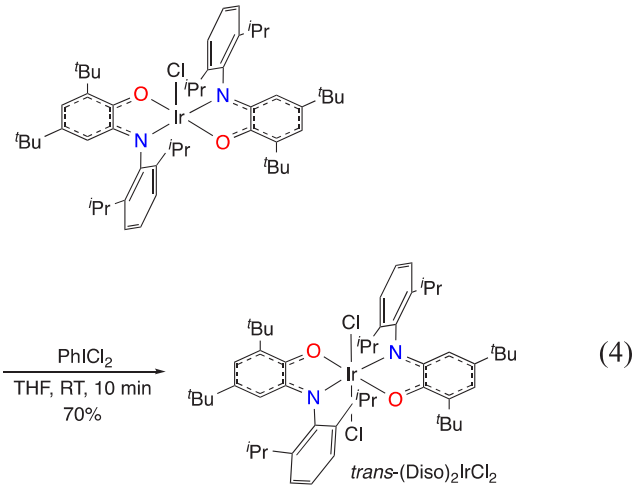


(4)

compound (Figure 5) adopts the *cis-α* configuration with the nitrogen atoms mutually *trans*, presumably for steric reasons. It has properties similar to the *trans* isomer (broad and moderately shifted $^1$H NMR signals, $\mu_{eff}$ = 1.60 $\mu_B$) but is distinct by $^1$H NMR (Figure S17) and by TLC on silica gel ($R_f$ = 0.12 vs 0.85 for the *cis* and *trans* compounds, respectively, in 2:1 dichloromethane/hexane). The two compounds do not interconvert readily. Heating the *trans* complex at 70 °C for a week in $CDCl_3$ shows no isomerization and heating at 100 °C for 2 d in $C_2D_2Cl_4$ leads to decomposition, while the *cis* complex can be heated at 100 °C for a week in $C_2D_2Cl_4$ without decomposition or isomerization. Electrochemically, the two isomers have similar cyclic voltammograms (Figure S7), with reversible one-electron oxidations ($E^\circ$ = 0.23 V vs $Cp_2Fe^+/Cp_2Fe$ for *trans*, 0.31 V for *cis*) and reversible one-electron reductions ($E^\circ$ = −0.58 and −0.51 V, respectively) at moderate potentials. The *cis* isomer's redox couples are shifted about 70 mV to more positive potentials compared to the *trans* isomer.

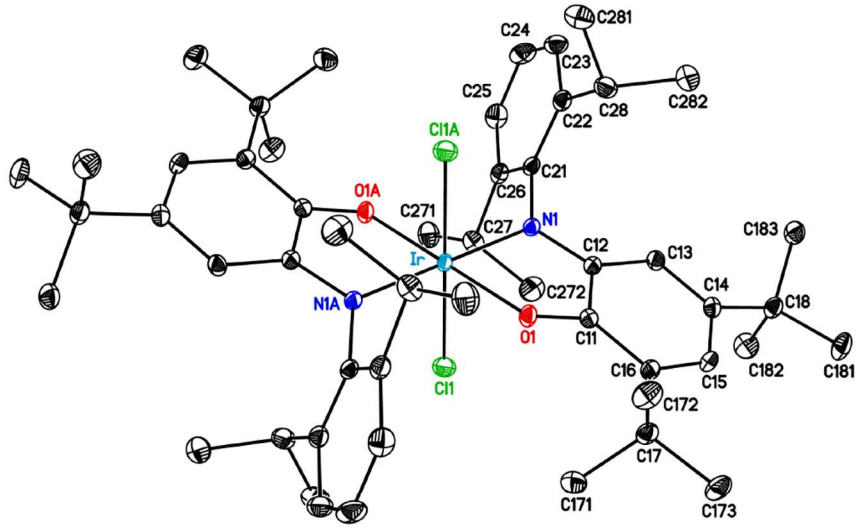


**Figure 4.** Thermal ellipsoid plot of *trans*-$(Diso)_2IrCl_2$. Hydrogen atoms are omitted for clarity.



https://doi.org/10.1021/acs.inorgchem.1c04005
Inorg. Chem. 2022, 61, 5547−5562

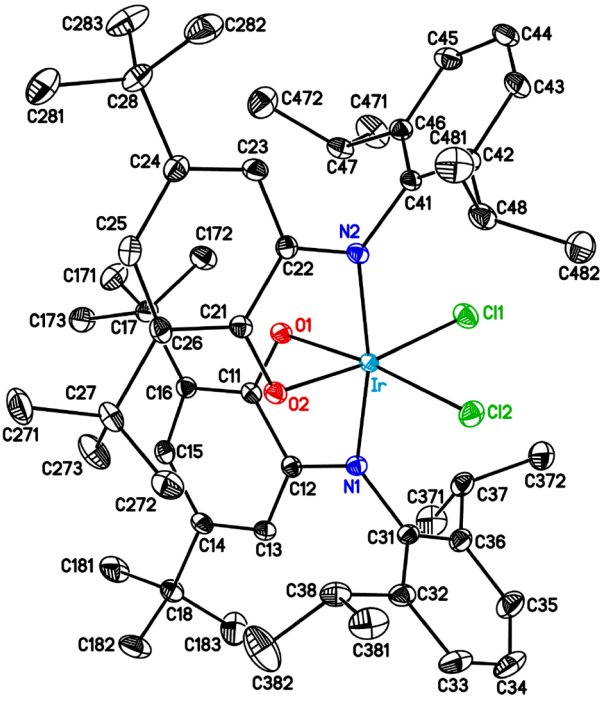


**Figure 5.** Thermal ellipsoid plot of *cis*-(Diso)$_2$IrCl$_2$. Hydrogen atoms are omitted for clarity.

Reduction of (Diso)$_2$IrCl with cobaltocene leads to formation of cobaltocenium chloride and the neutral, air-sensitive complex (Diso)$_2$Ir (eq 5), which adopts a square

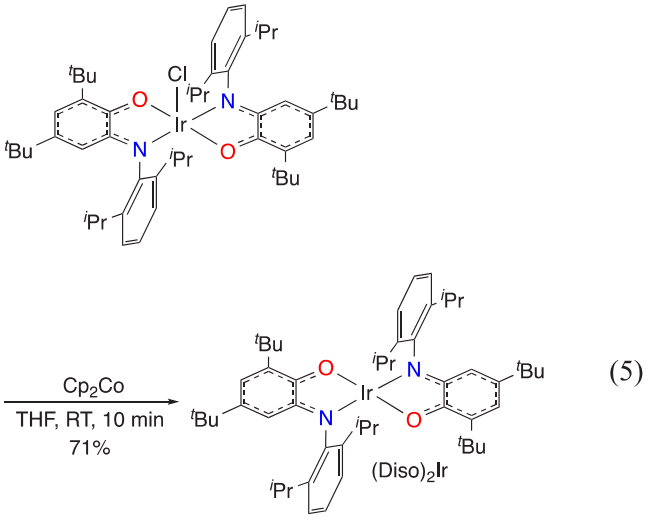


(5)

planar geometry (Figure 6). The paramagnetic complex shows a moderately broadened $^1$H NMR spectrum (Figure S18) and a solution magnetic moment ($\mu_{eff}$ = 1.59 $\mu_B$) consistent with an $S$ = 1/2 system.

**Electronic Structure of Monoiminoxolene Iridium Complexes.** The Cp*Ir(iminoxolene) complexes prepared by the groups of Rauchfuss[15,16] and Kaim[17] have been described as 16-electron complexes that show low Lewis acidity because of $\pi$ donation from the amidophenoxide ligand to iridium. DFT calculations (Figure 7a) confirm that the HOMO of CpIr(ap) (ap = *o*-C$_6$H$_4$(NPh)O) is predominantly composed of the iminoxolene RAO, consistent with the characterization of the ligand as an amidophenoxide in this complex. Some $\pi$ bonding is apparent, but it is limited by the fact that the d orbital into which the amidophenoxide can donate is $\sigma$* in character to the strongly donating cyclopentadienyl ligand. The low Lewis acidity is most likely principally due not to $\pi$ donation in the five-coordinate species, but rather to avoidance of a $\pi$* interaction that would be present in a pseudo-octahedral Lewis base adduct. The metrical data in the isolated Cp* complexes are consistent with at most modest $\pi$ donation, with metrical oxidation state (MOS) values of −1.72(6)[15] and −1.69(9)[17] only slightly lowered from the −2.00 expected for an amidophenoxide with negligible $\pi$ donation. Analyses of the isoelectronic complexes Cp*Ir(ArNCHCHNAr)[22] and (3,5-$^t$Bu$_2$Cat)Mn(CO)$_3$[23] are extremely similar.

Nominally, the cyclooctadiene and chloride ligands form an L$_2$X set[24] isoelectronic with cyclopentadienyl. However, the much weaker donor ability of (cod)Cl means that the $\pi$ interaction of iridium with the iminoxolene is stronger, an effect that is enhanced by a change in geometry from the two-legged piano stool of CpIr(ap) to the square pyramidal geometry of (ap)Ir(cod)Cl, which makes the relevant iridium $\pi$ orbital more nonbonding toward the (cod)Cl than it is to the Cp* ligand. DFT calculations (Figure 7b) suggest that there is iridium-iminoxolene $\pi$ bonding character in both the d$\pi$ orbital (HOMO−2) and the d$\sigma$* orbital (HOMO). Time-dependent DFT (TDDFT) calculations suggest that this gives rise to an optical spectrum with two strong absorptions in the visible region ($\lambda_{max}$ = 646 and 460 nm, Figure S19), compared to the single absorption in the blue region of the spectrum observed in Cp*Ir(iminoxolene) ($\lambda_{max}$ = 450−460 nm).[15−17]

Structurally, the strong iridium-iminoxolene $\pi$ bonding is manifested in the intraligand bond distances, which correspond to an iminoxolene MOS of −1.06(6) (Table 2). The redox plasticity of the iminoxolene, with a change in apparent oxidation state of over 0.65 on changing the ancillary ligand from Cp to (cod)Cl, is noteworthy. On the basis of the MOS, the iridium could be argued to have a nominal oxidation state of +2, but this picture has little to recommend it as a way of affording insight into the compound's structure and bonding. Iridium(II) is an uncommon oxidation state in monometallic compounds, and is most commonly seen in square planar complexes,[25,26] though five-coordinate compounds are also known.[27] A more chemically informative way of parsing the MOS value is to consider it as reporting on the electron density on the ligand in the RAO. The observed value thus reflects a filled $\pi$ orbital that is nearly equally shared between the iminoxolene ligand and the iridium.

**Electronic Structure of Bis-iminoxolene Iridium Monohalides.** The bis-iminoxolene complex (Diso)$_2$IrCl can be viewed formally as being related to the monoiminoxolene complex (Diso)Ir(cod)Cl by replacement of the neutral bidentate cyclooctadiene ligand by a neutral bidentate iminoquinone. In contrast to the monoiminoxolene complex, however, the bis-iminoxolene has two ligand-based RAOs that form *A*- and *B*-symmetry combinations in the $C_2$ symmetry of (Diso)$_2$IrX. These two combinations behave rather differently. In a square planar late-metal complex such as Pt(iminoxolene)$_2$,[9,11] the *B*-symmetry combination would have good overlap with a metal d$\pi$ orbital and would form a filled (largely metal-centered) $\pi$ bonding combination and an empty (largely ligand-centered) $\pi$* combination. The *A*-symmetry orbital is strictly nonbonding with respect to the metal and is filled. The existence of close-lying ligand-centered filled $\pi_{nb}$


https://doi.org/10.1021/acs.inorgchem.1c04005
Inorg. Chem. 2022, 61, 5547−5562

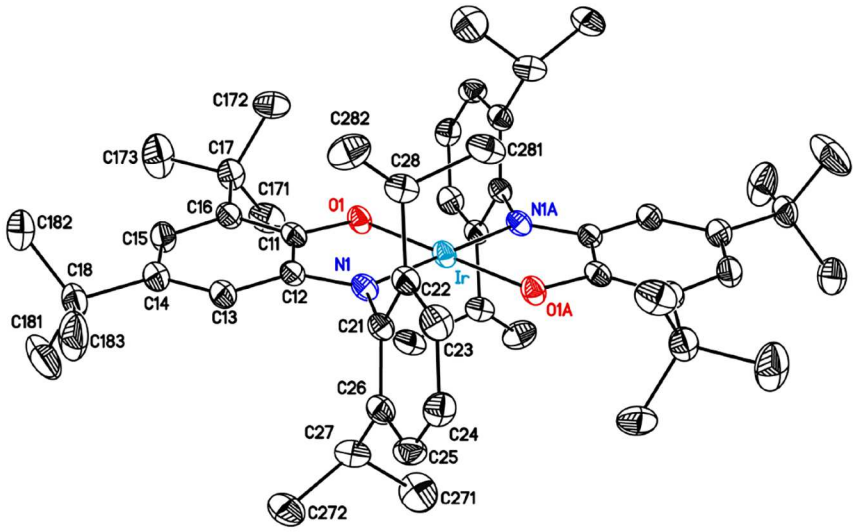


**Figure 6.** Thermal ellipsoid plot of $(Diso)_2Ir$. Hydrogen atoms have been omitted for clarity.

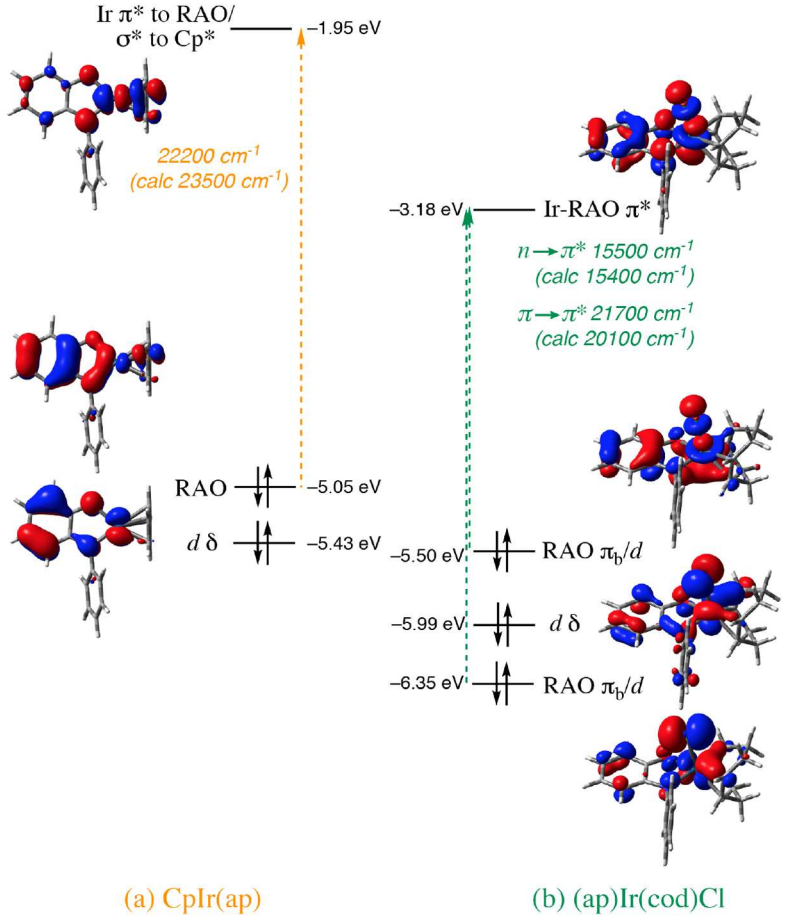


**Figure 7.** MO diagrams of (a) CpIr(ap) and (b) (ap)Ir(cod)Cl.

and empty $\pi^*$ orbitals has led to a description of the square planar group 10 compounds as bis(iminosemiquinones) containing strongly coupled radicals, with an open-shell singlet ground state characterized by substantial configuration interaction.[28] In the platinum congeners, the bonding interaction is sufficiently strong that the physical markers of the open-shell singlet (such as a low-lying triplet state) are absent, indicating very strong coupling and a small amount of configuration interaction.[11]

Two factors cause the bonding description in $(Diso)_2IrX$ to deviate from that of $Pt(iminoxolene)_2$. The first is the lower electronegativity of the central metal in the iridium complex. This brings the metal d orbitals closer in energy to the iminoxolene RAOs, which increases the covalency of the


https://doi.org/10.1021/acs.inorgchem.1c04005
Inorg. Chem. 2022, 61, 5547−5562

Table 2. Selected Bond Distances (Å) and Metrical Oxidation States[20] for (Diso)Ir(cod)Cl·0.5 $CH_3CN$, $(Diso)_2IrCl·3C_6H_6$, $(Diso)_2IrI·C_3H_6O$, $(Diso)_2Ir$, *trans*-$(Diso)_2IrCl_2$, and *cis*-$(Diso)_2IrCl_2$

| | (Diso)Ir(cod)Cl·0.5$CH_3CN$ | $(Diso)_2IrCl·3C_6H_6$ | $(Diso)_2IrI·C_3H_6O$[a] | $(Diso)_2Ir$ | *trans*-$(Diso)_2IrCl_2$ | *cis*-$(Diso)_2IrCl_2$[a] |
|---|---|---|---|---|---|---|
| Ir−O | 2.0352(10) | 2.0065(14) | 2.008(7) | 1.964(2) | 2.0055(12) | 2.020(4) |
| Ir−N | 2.0077(12) | 1.9424(18) | 1.929(16) | 1.941(3) | 2.0064(15) | 2.0165(11) |
| Ir−X (X = Cl, I) | 2.3966(4) | 2.3136(7) | 2.609(5) | | 2.3413(5) | 2.3135(14) |
| O−C11 | 1.3036(18) | 1.313(2) | 1.311(12) | 1.341(4) | 1.300(2) | 1.304(3) |
| N−C12 | 1.3610(18) | 1.369(3) | 1.387(16) | 1.380(4) | 1.340(2) | 1.3427(19) |
| C11−C12 | 1.430(2) | 1.415(4) | 1.418(15) | 1.415(4) | 1.450(2) | 1.444(5) |
| C12−C13 | 1.416(2) | 1.411(3) | 1.402(16) | 1.397(5) | 1.417(2) | 1.417(3) |
| C13−C14 | 1.369(2) | 1.373(3) | 1.370(13) | 1.387(5) | 1.369(2) | 1.366(2) |
| C14−C15 | 1.431(2) | 1.420(3) | 1.418(14) | 1.419(5) | 1.434(3) | 1.432(4) |
| C15−C16 | 1.373(2) | 1.385(3) | 1.380(15) | 1.389(5) | 1.376(3) | 1.377(3) |
| C16−C11 | 1.431(2) | 1.426(3) | 1.426(13) | 1.413(5) | 1.431(2) | 1.426(3) |
| MOS | −1.06(6) | −1.27(8) | −1.32(11) | −1.55(6) | −0.88(2) | −0.94(3) |

[a]Metrical data are averaged among chemically equivalent values, with stated esd's reflecting both the variance in the measured values and the statistical uncertainty of the crystallographic model.

metal−ligand $\pi$ interaction. Thus, the *B*-symmetry $\pi$ bonding orbital (Figure 8; HOMO−3 for $(ap)_2IrCl$, HOMO−2 for $(ap)_2IrI$, Figure 9), while still preponderantly metal-based, has a sizable contribution from the ligand RAOs, and the *B*-symmetry $\pi^*$ orbital (Figure 8; LUMO, Figure 9) has a sizable metal contribution.

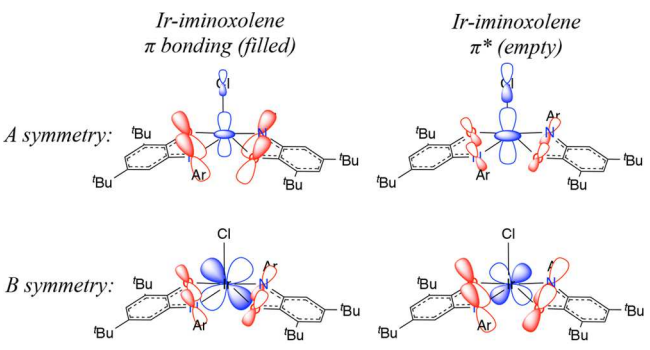


**Figure 8.** Qualitative description of Ir-iminoxolene $\pi$ interactions in $(Diso)_2IrCl$. Only the contributions from the metal and first coordination sphere atoms are shown.

The second factor is the change in geometry from square planar to square pyramidal. This allows for $\pi$ overlap between the *A*-symmetry RAO combination and the iridium $dz^2$ orbital. Since the latter orbital is $\sigma^*$ with respect to the halide, it is relatively high in energy, so the filled $\pi$ bonding combination is largely ligand-centered (Figure 8; HOMO, Figure 9) and the $\pi^*$ combination is largely metal-centered (Figure 8; LUMO+1, Figure 9). The $\sigma^*$ character of the LUMO+1 orbital makes it sensitive to the identity of the halide, with the more weakly bonded iodide having the lower-energy orbital (Figure 9). (A similar halide dependence is seen in the *B*-symmetry $\pi$ bonding orbital, which is predicted to be noticeably higher in energy for the iodide complex by DFT, presumably because this orbital has metal−halogen $\pi^*$ character.) The effect of the halogen is borne out by optical spectroscopy (Figure 10). TDDFT calculations predict that the visible spectra will be dominated by intense transitions assigned as $\pi(A) \rightarrow \pi^*(B)$ at low energy and $\pi(B) \rightarrow \pi^*(A)$ at higher energy. The former is predicted and observed to be insenstive to the identity of the halogen, while the latter is predicted to shift by 1900 $cm^{-1}$ (and

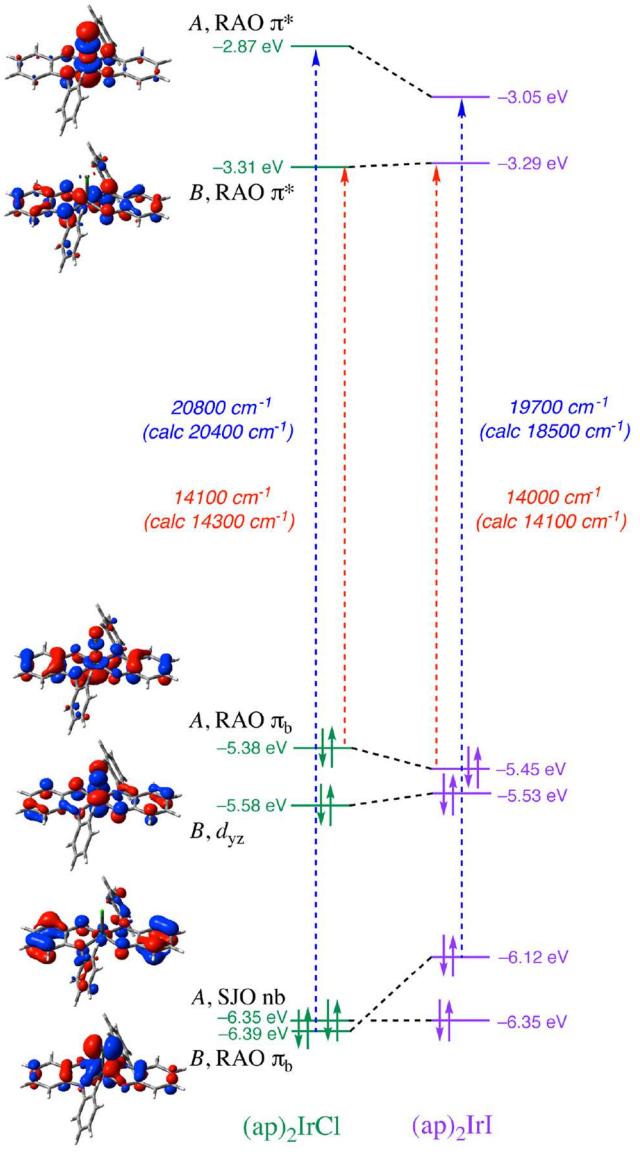


**Figure 9.** Molecular orbital diagram of $(ap)_2IrCl$ and $(ap)_2IrI$. Kohn−Sham orbitals are illustrated for the chloride complex.



https://doi.org/10.1021/acs.inorgchem.1c04005
Inorg. Chem. 2022, 61, 5547−5562

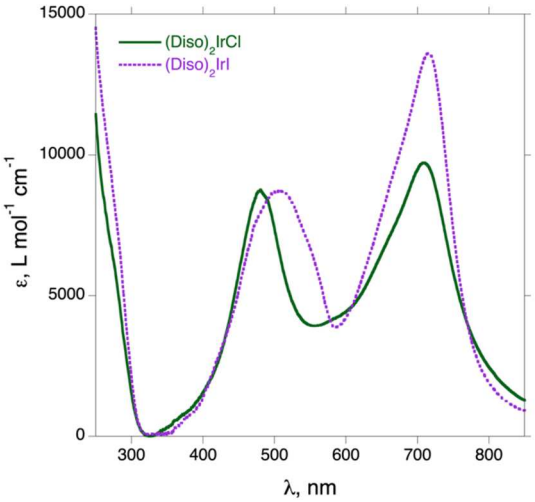


**Figure 10.** Optical spectra of $(Diso)_2IrX$ (X = Cl, solid line; X = I, dotted line) in $CH_2Cl_2$.

observed to shift by 1100 $cm^{-1}$) to a lower energy on substitution of chloride by iodide.

**Electronic Structure of Paramagnetic Bis-(iminoxolene)iridium Complexes.** Square planar $(Diso)_2Ir$ has the same electron count as cationic group 10 complexes $(iminoxolene)_2M^+$ (M = Ni, Pd, Pt), whose electronic structures have been well studied.[10,11] In the group 10 compounds, the unpaired electron resides in a purely ligand-centered $A_u$ orbital, giving rise to intense LLCT absorptions in the near-IR ($\lambda_{max}$ = 1530 nm for $(Snip)_2Pt^+$, Snip = *N*-(3,5-di-*tert*-butylphenyl)-4,6-di-*tert*-butyl-*o*-iminobenzoquinone)[11] and nearly isotropic *g* values near the free electron value of 2.0023 in the EPR (*g* = 1.937, 1.997, 2.012 for $(^{Ph}ap)_2Pt^+$, $^{Ph}ap$ = *N*-phenyl-4,6-di-*tert*-butyl-*o*-iminobenzoquinone).[9]

The spectroscopic features of $(Diso)_2Ir$ are not consistent with those of $(^{Ph}ap)_2Pt^+$. In particular, the optical spectrum shows intense absorption in the visible rather than the near-IR (Figure 11), and the EPR spectrum is both highly anisotropic and has an average *g* value significantly different from that of the free electron (Figure 12, *g* = 1.7267, 1.9001, and 3.6343).

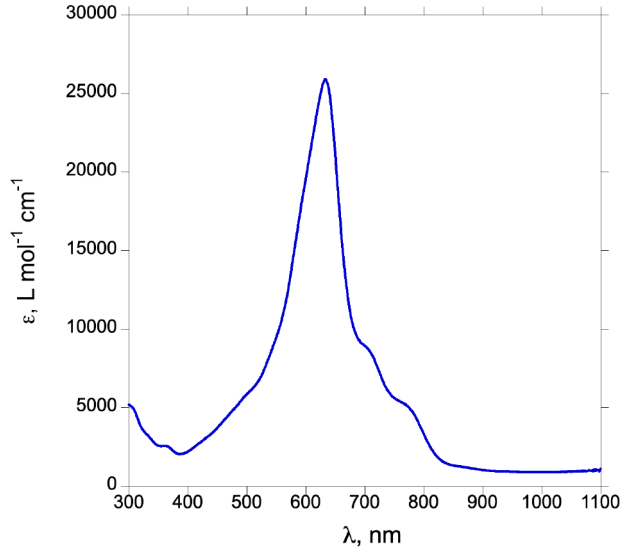


**Figure 11.** Optical spectrum of $(Diso)_2Ir$ (in $CH_2Cl_2$).

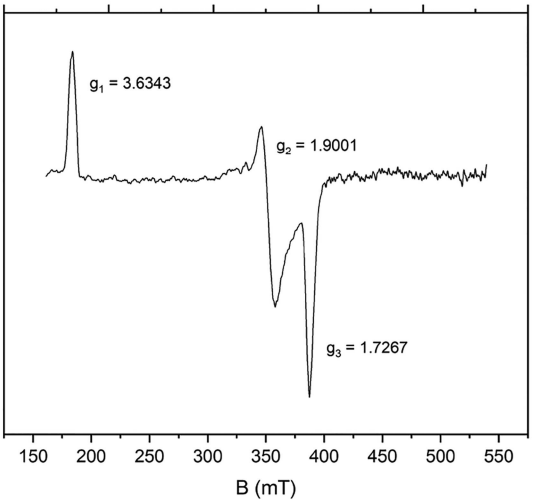


**Figure 12.** EPR spectrum of $(Diso)_2Ir$ (X-band, 10 K, toluene glass).

This indicates that the unpaired electron is in a metal-centered, rather than a ligand-centered, orbital. The EPR features are similar to those reported for square planar iridium(II) compounds with $\pi$ donor ligands such as alkoxides or amides.[26] The spectroscopic observations are consistent with the results of DFT calculations (Figure 13a), which suggest that the unpaired electron is in an orbital that is principally iridium $d_{yz}$ in character. While the d orbitals of the group 10 metals are significantly lower in energy than the ligand RAOs, the iridium orbitals are higher in energy, and $d_{yz}$ in particular is raised in energy through its $\pi^*$ interaction with the iminoxolene subjacent orbital (SJO, the out-of-phase $\pi$ lone pair orbital). Such $\pi$ interactions have been shown to have significant effects in osmium and ruthenium complexes,[29] and square planar iridium(II) radicals have been noted to have a preference for placing the odd electron in a d$\pi$ orbital rather than the $d_{z^2}$ orbital.[25e] Thus, while the group 10 metal orbitals are sufficiently far below the RAOs to ensure that they exert only a modest perturbation on a ligand-centered system, the metal orbitals in $(Diso)_2Ir$ are sufficiently close to the ligand orbitals that they cannot be ignored. The orbital picture shown here is qualitatively the same as that previously calculated for isoelectronic $(C_6H_4[NH]_2)_2Co$.[30]

On moving from $(Diso)_2Ir$ to *trans*-$(Diso)_2IrCl_2$, these orbital energies are significantly affected. Addition of two electron-withdrawing chlorine atoms is expected to lower the energy of the iridium d orbitals (except, of course, for the newly $\sigma^*$ $d_{z^2}$ orbital, which loses its two electrons to account for the overall two-electron oxidation of the compound). There is thus a substantial drop in the energy of the $d_{yz}$ orbital that was singly occupied in $(Diso)_2Ir$ ($B_g$ Ir-SJO $\pi^*$, Figure 13). At the same time, the strictly nonbonding $A_u$ RAO orbital is calculated to rise appreciably in energy. This phenomenon is likely due to the change in bond lengths in the ligand, where the more positive MOS in *trans*-$(ap)_2IrCl_2$ (calculated to be −0.84(6) vs −1.60(7) in $(ap)_2Ir$) reflects a structure where filling the RAO is less energetically favorable, as has been invoked to explain the more facile oxidation of ruthenium tris(iminoxolenes) compared to their osmium analogues.[13] These two effects combine to place the ligand-centered $A_u$ orbital substantially above the metal-based $B_g$ orbital, giving rise to a ligand-centered SOMO. The *cis* isomer has a similar electronic structure, despite the fact that in the *cis* geometry


https://doi.org/10.1021/acs.inorgchem.1c04005
Inorg. Chem. 2022, 61, 5547−5562

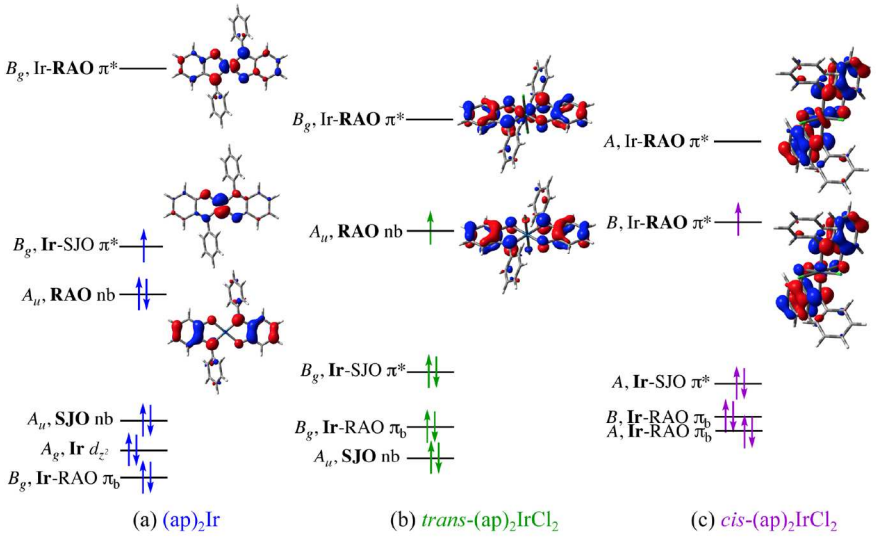


**Figure 13.** Qualitative MO diagrams of (a) $(ap)_2Ir$, (b) *trans*-$(ap)_2IrCl_2$, and (c) *cis*-$(ap)_2IrCl_2$. Orbital energies are positioned according to the average energy of the Kohn−Sham $\alpha$ and $\beta$ spin orbitals. Illustrations of the frontier orbitals are of the Kohn−Sham $\beta$ spin orbitals. The predominant contributors to the orbitals (Ir or ligand RAO or SJO) are shown in boldface.

both RAO combinations can overlap with metal d$\pi$ orbitals, because the iminoxolene ligand can pivot to minimize the overlap of the *B*-symmetry combination with the d$\pi$ orbital, weakening the antibonding interaction. In osmium and ruthenium compounds where this orbital is occupied, typical X−M−N1−C12 dihedral angles are about 115°, compared to the ∼70° dihedral angles seen in compounds where the orbital is empty and hence greater overlap leads to enhanced bonding.[31] The values observed experimentally in *cis*-$(Diso)_2IrCl_2$ (104.5° avg) and computationally in *cis*-$(ap)_2IrCl_2$ (93.6°) are intermediate between these two extremes, as expected for a compound where this orbital is singly occupied and indicates that this orbital is weakly Ir-iminoxolene $\pi$ antibonding in character.

Experimentally, the optical and EPR spectra of both isomers of $(Diso)_2IrCl_2$ contrast with the properties of $(Diso)_2Ir$ and are consistent with principally ligand-centered SOMOs. The compounds both show intense and relatively narrow transitions in the near-IR region (Figure 14), as is seen for the group 10 bis(iminoxolene) cations. The *cis* isomer shows somewhat lower energy, and markedly less intense bands, than does the *trans* isomer. The EPR spectra (Figure 15) show no discernible *g* value anisotropy and *g* values close to 2, typical of organic radicals.

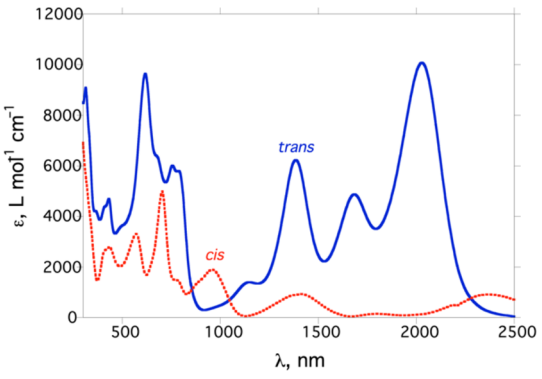


**Figure 14.** UV−visible-NIR spectra (in $CCl_4$) of *trans*-$(Diso)_2IrCl_2$ (solid line) and *cis*-$(Diso)_2IrCl_2$ (dotted line).

## DISCUSSION

**On the Covalency of the Iridium-Iminoxolene $\pi$ Interaction.** One way of parsing the bonding in compounds of redox-active ligands such as iminoxolenes is to assign electrons as either metal-localized or ligand-localized, giving integer oxidation states. The electronic and magnetic properties can then be interpreted in terms of coupling between metal- or ligand-centered radicals. This model is strictly correct in the limit of purely ionic bonding, where by definition electrons must be localized on either the metal or the ligand. It is therefore unsurprising that this approach has been most successful in compounds with largely ionic bonding, such as first-row metal complexes of catecholate ligands.[2] Iminoxolene complexes of group 10 metals, where the metal d orbitals are low enough in energy that they have only modest interactions with the ligand RAOs, have also been successfully described using this model.[9−11]

In complexes of iminoxolenes with second- and third-row transition metals from the middle of the d block, covalency is high because of good spatial overlap and energy match between the metal d orbitals and the ligand RAOs. For these compounds, the ionic model becomes awkward or even misleading, and compounds are more sensibly understood not in terms of assigned oxidation states, but rather using molecular orbital descriptions featuring strong, covalent metal-iminoxolene $\pi$ interactions. Iminoxolene complexes of the group 8 metals ruthenium and osmium are exemplars of this description, with the composition of the metal-iminoxolene bonding orbitals for the two metals straddling equal-sharing covalency (∼65% metal-centered for Ru and ∼40% metal-centered for Os).[13]

The results of the present study indicate that iridium iminoxolene complexes are generally better understood by the covalent model than the ionic model. Three characteristic observations support this conclusion. The first is that there is a generally poor correspondence between structurally defined oxidation states (MOS) and chemically reasonable integer


https://doi.org/10.1021/acs.inorgchem.1c04005
Inorg. Chem. 2022, 61, 5547−5562

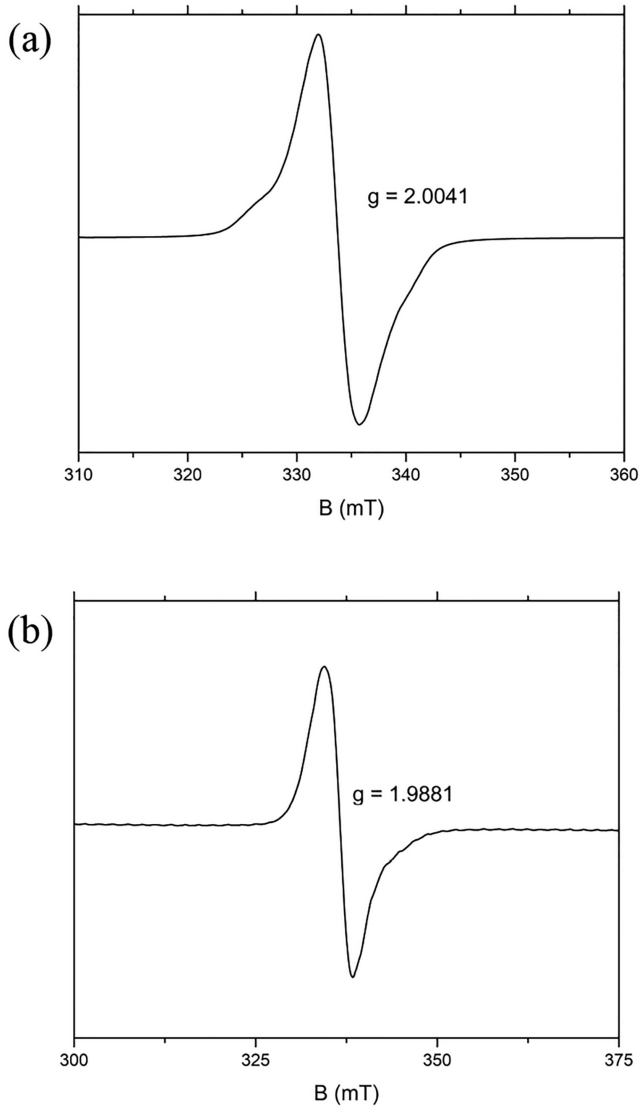


**Figure 15.** EPR spectra of (a) *trans*-$(Diso)_2IrCl_2$ and (b) *cis*-$(Diso)_2IrCl_2$. Conditions: X-band, 10 K, $CH_2Cl_2$ glass.

oxidation states (Table 3). For example, neither $(Diso)_2IrCl$ (MOS = −1.27(8)) nor *trans*-$(Diso)_2IrCl_2$ (MOS = −0.88(2)) correspond well to any whole number of electrons on the iminoxolene ligands. The appearance of fractional MOSs is an established hallmark of the presence of significant $\pi$ bonding.[20] Even when the metal oxidation states corresponding to the structural data are integers within experimental error, the apparent oxidation state is often not chemically reasonable. (Diso)IrCl(cod) has an apparent metal oxidation state near +2, but as discussed above, assigning this compound as Ir(II) is chemically unappealing. Assigning the iridium center in $(Diso)_2Ir$ as the metrically appropriate Ir(III) state is similarly unpalatable, requiring a rare square-planar geometry[26b] (four-coordinate iridium(III) is highly uncommon, and typically adopts a *cis*-divacant octahedral geometry[32,33]). In these cases, an interpretation invoking nearly equal-sharing covalent $\pi$ bonding is a more sensible way of rationalizing the observed structural data.

A second observation favoring a covalent bonding model is the extreme redox plasticity of the ligands in response to changes in ancillary ligation. In a (polar) covalent model of $\pi$ bonding, the degree of localization of the metal-iminoxolene $\pi$ bonding orbital is expected to be tuned by changes in the energy (and possibly overlap) of the metal d$\pi$ orbital participating in the bonding. For example, bis(iminoxolene) osmium complexes $(^{H}ap)_2Os(OCH_2CH_2O)$ and $(^{H}ap)_2OsCl_2$ have ligand MOS values that differ by more than 0.5 units, which is most plausibly interpreted as resulting from $\pi$ donation from the alkoxide ligands raising the energy of the osmium d$\pi$ orbitals.[14] In the iridium compounds, a similar effect engendered by differences in $\sigma$ bonding is observed in the difference between Cp*Ir(iminoxolene) (MOS = −1.71 avg.) and (Diso)IrCl(cod) (MOS = −1.06(6)).

A final observation relevant to the degree of covalency of the metal-iminoxolene interaction is the structural response of the complex to oxidation or reduction. If the bonding is principally ionic, oxidation of the compound by one electron should result in a change in overall iminoxolene MOS of either +1 unit (if the oxidation is ligand-centered) or 0 units (if the oxidation is metal-centered). If the bonding is substantially covalent, then oxidation would result in a fractional change in MOS, with the fraction reflecting the distribution of the electron density between ligand and metal in the relevant orbital. For example, the change of +0.94 in MOS on going from neutral $Cp^*Ir(^{CF3}ap)$ (MOS = −1.72(7)) to cationic $[Cp^*Ir(^{CF3}ap)]^+$ (MOS = −0.78(8)) is consistent with a ligand-localized oxidation in this compound,[15] congruent with the compound's HOMO being largely localized on the ligand (Figure 7a). In the bis(iminoxolene) series, the simplest sequence of oxidation states is found in $(Diso)_2IrCl_n$ ($n$ = 0, 1, or 2, Table 3). The changes in MOS on going from $(Diso)_2Ir$ to $(Diso)_2IrCl$ (+0.56 total among the two iminoxolenes) and from $(Diso)_2IrCl$ to *trans*-$(Diso)_2IrCl_2$ (+0.78) are both significantly

**Table 3. Metrical Parameters for Group 9 Iminoxolene Complexes**

| compound[a] | $N$ | M−O (Å) | M−N (Å) | iminoxolene MOS | apparent metal oxidn. state | refs |
|---|---|---|---|---|---|---|
| $Cp^*Ir(io)$ | 2 | 2.003(10) | 1.955(12) | −1.71(2) | +2.71 | 15, 17 |
| (Diso)IrCl(cod) | 1 | 2.0352(10) | 2.0077(12) | −1.06(6) | +2.06 | this work |
| $(Diso)_2Ir$ | 1 | 1.964(2) | 1.941(3) | −1.55(6) | +3.10 | this work |
| $(Diso)_2IrCl$ | 1 | 2.0065(14) | 1.9424(18) | −1.27(8) | +3.54 | this work |
| *trans*-$(Diso)_2IrCl_2$ | 1 | 2.0055(12) | 2.0064(15) | −0.88(2) | +3.76 | this work |
| $(io)_2Co$ | 6 | 1.825(3) | 1.839(5) | −1.36(7) | +2.72 | 30, 34−36 |
| $(io)_2CoX$[b] | 13 | 1.866(7) | 1.859(7) | −0.89(4) | +2.78 | 35−37 |
| $(io)_2Co(EPh)$[c] | 3 | 1.859(5) | 1.855(2) | −1.05(2) | +3.10 | 36 |
| $(io)_2Co(CH_2R)$ | 3 | 1.857(10) | 1.855(5) | −1.12(7) | +3.24 | 30, 38 |
| $(io)_3Co$ | 7 | 1.890(6) | 1.927(6) | −0.98(3) | +2.94 | 39 |

[a]io = iminoxolene. [b]X = halide or pseudohalide. [c]E = S or Se.



https://doi.org/10.1021/acs.inorgchem.1c04005
Inorg. Chem. 2022, 61, 5547−5562

<1.0. While this is consistent with both the ligand and the metal sharing in the oxidation, the situation is complicated by the changes in electronic structure among the three compounds. In $(Diso)_2Ir$ and $(Diso)_2IrCl$, both the *A*-symmetry and *B*-symmetry RAO-based orbitals are filled, while in *trans*-$(Diso)_2IrCl_2$, the $A_u$-symmetry orbital is singly occupied. The simplest comparison is actually the two-electron couple $(Diso)_2Ir$/*trans*-$(Diso)_2IrCl_2$, where the $A_u$ orbitals are strictly nonbonding, while the filled $B_g$ orbitals are metal-iminoxolene $\pi$ bonding. Based on the change in occupancy of the $A_u$ orbital, one would expect a change in MOS of +0.50; the observed change is +0.67. The additional apparent ligand oxidation is consistent with the bonding orbital becoming more metal-centered in the oxidized compound. Since the $A_u$ orbitals are strictly ligand-centered by symmetry, one can calculate the apparent distribution of the $B_g$ $\pi$ bonding orbitals from the overall MOS as being 45% iridium-centered in $(Diso)_2Ir$ but 62% iridium-centered in *trans*-$(Diso)_2IrCl_2$.

In comparing $(Diso)_2Ir$ to $(Diso)_2IrCl$, the occupancy of the orbitals is unchanged, so the entire 0.39 change in MOS must be due to changes in the distribution of electrons in the two occupied RAO-based orbitals. Some of this is presumably due to the presence of the additional chloride in $(Diso)_2IrCl$, but from the above analysis, this would be expected to account only for a small amount of the overall change. Another major change is that the *A*-symmetry orbital is no longer strictly ligand-centered. Given the appreciable pyramidalization in the structure, there is good overlap between this orbital and the iridium $dz^2$ orbital, and significant metal character is observed in the filled orbital (Figure 9, HOMO). Assuming that the composition of the *B*-symmetry $\pi$ bonding orbital is intermediate between that observed in $(Diso)_2Ir$ and *trans*-$(Diso)_2IrCl_2$ (~53% Ir-centered), this implies ~80% ligand character in the *A* orbital, in qualitative agreement with the MO calculations.

Thus, the occupied *B* combinations involving the ligand RAOs in the iridium bis(iminoxolenes) are concluded to be highly covalent, with metal character from 45 to 60% depending on the ancillary ligands. The 62% iridium character of the bonding orbital in *trans*-$(Diso)_2IrCl_2$ is similar to the 66% metal character in bonding orbitals in octahedral ruthenium iminoxolenes,[13] as expected given the two elements' diagonal relationship.

**Implications of Covalency in First-Row Metal Iminoxolene Complexes.** Much has been made of the ability of redox-active ligands to allow first-row transition metals to participate in the two-electron redox events more common in second- and third-row metals.[40] The present work illustrates the inverse property, namely the ability of such ligands to enable stable compounds separated by one-electron redox events to be formed from the second- or third-row late transition metals. One of the most striking aspects of the chemistry of $(Diso)_2IrCl$ is its amenability to such single-electron redox events. Removal of a chlorine atom—a one-electron reduction—produces stable $(Diso)_2Ir$, while addition of a chlorine atom—a one-electron oxidation—affords stable $(Diso)_2IrCl_2$. (In contrast to these inner-sphere redox events, outer-sphere redox chemistry of these compounds is not always well-behaved. $(Diso)_2Ir$ and $(Diso)_2IrCl$ show only irreversible waves in their cyclic voltammograms [Figures S5 and S8], though both isomers of $(Diso)_2IrCl_2$ show reversible oxidations and reductions [Figure S7].) The iminoxolene ligands have evidently overridden iridium's preference for undergoing two-electron oxidation-state changes.

In this context, it is worth comparing the iridium compounds to their cobalt congeners. A number of four-coordinate $(iminoxolene)_2Co$ complexes have been prepared, and with the exception of tetrahedral $(C_6H_2\text{-}4,6\text{-}{}^tBu_2\text{-}2\text{-}(N^tBu)\text{-}O)_2Co$,[41] their structural (square planar geometry) and spectroscopic properties (e.g., highly anisotropic EPR spectra) parallel those of $(Diso)_2Ir$. A detailed study concluded that for the cobalt compounds, "spectroscopic oxidation states describing a $d^6$ ($Co^{III}$) or $d^7$ ($Co^{II}$) electron configuration cannot be unambiguously assigned"[30] and proposed an electronic structure analogous to that described here for $(Diso)_2Ir$. The MOS values of these compounds (−1.36(7) average, Table 3) are consistent with such a covalent description and suggest that the cobalt-iminoxolene bonding orbital has ~64% cobalt character.

The diamagnetic five-coordinate compounds $(iminoxolene)_2CoX$ have generally been assigned as containing low-spin Co(III) with strongly antiferromagnetically coupled iminosemiquinone radicals.[30,34,35] This is in reasonable agreement with the metrical data (average MOS for pseudohalide complexes = −0.89(4), Table 3). However, the structural (square pyramidal geometry) and spectroscopic (presence of two intense bands in the visible region) similarities between the cobalt compounds and their iridium congeners strongly suggest that the same bonding description applies to both types of compounds. This in turn suggests that covalency plays an important role in the bonding of the cobalt compounds as well. Foregrounding the covalency of the cobalt-iminoxolene interaction helps to explain the structural features of the compounds, in particular the noticeably more negative values of the ligand MOS as the electronegativity of the axial ligand decreases (Table 3, X = pseudohalide vs thiolate/selenolate vs alkyl). This structural plasticity depending on the ancillary ligands is difficult to rationalize in the ionic formulation, but is readily rationalized based on a decrease in cobalt character in the occupied (bonding) metal-iminoxolene $\pi$ orbitals.

The description of the electronic structure of $(iminoxolene)_2MX$ as having a M(III) ion with antiferromagnetically coupled ligands is not incorrect, but in cases where the antiferromagnetic coupling constants are extremely large, using the language of polyradicals to describe the compounds runs the risk of glossing over key aspects of the bonding. The large antiferromagnetic coupling must have its origin in chemical bonding, in this case the difference in overlap between the *A*- and *B*-symmetry RAO combinations and the cobalt $d\pi$ orbitals. The language of antiferromagnetically coupled diradicals suggests an approximate description of the molecule as having (uncoupled) radicals, with their coupling appended as a perturbation, while the language of covalency foregrounds the importance of bonding interactions at the expense of minimizing the importance of the configuration interaction that is characteristic of coupled diradicals. Neither verbal shorthand can thus be entirely satisfactory for these strongly coupled diradicals. It is not surprising that compounds of the third-row transition metals, with their characteristically strong bonding, will require a consideration of the covalency of the metal-iminoxolene $\pi$ interactions to satisfactorily describe their electronic structure. The similarity of $(iminoxolene)_2CoX$ to $(Diso)_2IrX$ suggests that even in the first-row transition-metal compounds, the covalency of the iminoxolene-metal interaction cannot be neglected. The difference is that the weaker


https://doi.org/10.1021/acs.inorgchem.1c04005
Inorg. Chem. 2022, 61, 5547−5562

bonding in the first-row transition-metal compounds allows the possibility of compounds with minimal covalency. Thus, tris(iminoxolene) cobalt complexes, with their longer Co-ligand bonds, give MOSs very close to −1 (Table 3) and are well described as triradicals with weak coupling between the ligand spins.[39] Iridium tris(iminoxolene) complexes, which would require the population of orbitals with strongly metal−ligand $\pi$ antibonding interactions,[13] have never been observed.

The ability of redox-active ligands to "ennoble" first-row and early transition metals has usually been ascribed to their ability to act as electron reservoirs in redox reactions.[40] This is undoubtedly critical in allowing redox reactions of early or late transition metals that would normally form redox-inactive compounds.[42] But the present work suggests that in the middle of the transition series, an equally or more important factor may be the covalency of the metal−ligand interaction. This is a familiar phenomenon in organometallic and coordination chemistry. It is well-known that organometallic complexes, with strong-field ligands such as carbonyls that form highly covalent bonds, show much more similarity within a group than do coordination compounds (thus, $Cr(CO)_6$ is rather similar to $Mo(CO)_6$ while $CrCl_3$ is not especially similar to $MoCl_3$). This effect leads to an attenuation of the physical significance of the oxidation state in organometallic compounds.[43] In the case of the bis(iminoxolene) complexes of the group 9 metals discussed here, the delocalization of the metal-iminoxolene bonding apparently allows the first- and third-row metal complexes to converge on a common electronic structure with common properties.

## CONCLUSIONS

Reaction of the iminoquinone Diso (*N*-(2,6-diisopropylphenyl)-3,5-di-*tert*-butyl-*o*-iminobenzoquinone) with iridium(I) precursors is a general route to iridium iminoxolene complexes. Reaction with $[(cod)IrCl]_2$ affords the mono-iminoxolene complex (Diso)Ir(cod)Cl, while the cyclooctene complex $[(coe)_2IrCl]_2$ gives the bis-iminoxolene complex $(Diso)_2IrCl$. In the latter complex, there is a strong $\pi$ interaction between the *B*-symmetry combination of ligand RAOs and the iridium $d_{xz}$ orbital and a weaker but still significant interaction between the *A*-symmetry RAO combination and the iridium $dz^2$ orbital. $(Diso)_2IrCl$ readily undergoes one-electron oxidation or reduction reactions. Reduction by cobaltocene yields square planar $(Diso)_2Ir$, while oxidation by $PhICl_2$ gives *trans*-$(Diso)_2IrCl_2$ (the *cis* isomer is available in low yield by air oxidation of $(Diso)_2IrCl$ and does not interconvert with the *trans* isomer). Since both $(Diso)_2Ir$ and *trans*-$(Diso)_2IrCl_2$ have $C_{2h}$ symmetry, the $A_u$-symmetry RAO combination is strictly nonbonding. It is filled in the square planar complex (with the odd electron residing in an orbital that is mostly Ir $d_{yz}$ in character) and singly occupied in the octahedral complex. In all cases, the strongly iridium-iminoxolene $\pi$ bonding orbitals are filled and are highly covalent, with structural data suggesting that they are about 45−60% metal in character, depending on the ancillary ligands. This covalency makes the assignment of the oxidation state of the metal both problematic and not especially useful. The spectroscopic and structural similarity of $(Diso)_2Ir$ and $(Diso)_2IrCl$ to their known cobalt congeners suggests a common bonding description, with the covalency of the metal-iminoxolene bonding serving to foster a convergence of the properties of the first- and third-row metal complexes.

## EXPERIMENTAL SECTION

**General Procedures.** Unless otherwise noted, all procedures were carried out in a drybox under a nitrogen atmosphere. *N*-(2,6-Diisopropylphenyl)-3,5-di-*tert*-butyl-*o*-iminobenzoquinone (Diso),[18] $[(coe)_2IrCl]_2$,[44] and $PhICl_2$[45] were prepared according to literature procedures. Dried solvents were purchased from Acros Organics and were stored in a nitrogen-filled drybox until use. Deuterated solvents (Cambridge Isotope Laboratories) were dried and vacuum transferred away from the drying agents and were stored in the drybox prior to use. $CD_2Cl_2$ and $CDCl_3$ were dried over 4 Å molecular sieves, followed by $CaH_2$. $C_6D_6$ and $C_6D_5CD_3$ were dried over sodium and tetrahydrofuran-$d_8$ over sodium benzophenone ketyl. NMR spectra were measured on a Bruker Avance DPX 400 or 500 MHz spectrometer. Chemical shifts for $^1H$ and $^{13}C\{^1H\}$ spectra are reported in ppm downfield of TMS, with spectra referenced using the known chemical shifts of the solvent residuals. Infrared spectra of air-stable compounds were recorded by ATR on a Jasco 6300 FT-IR spectrometer and are reported in wavenumbers. For air-sensitive compounds, infrared spectra were taken of nujol mulls prepared in the drybox and pressed between NaCl discs. UV−vis-NIR spectra were recorded in 1 cm quartz cells on a ThermoFisher Evolution Array diode array spectrophotometer, an Agilent 8453 diode array spectrophotometer, or a Jasco V-670 spectrophotometer. Elemental analyses were performed by M-H-W Laboratories (Phoenix, AZ, USA) or Midwest Microlabs (Indianapolis, IN, USA). Magnetic moments were determined by the Evans method[46] using 1,4-bis(trimethylsilyl)benzene as the reference compound as previously described.[47]

**(Diso)Ir(cod)Cl.** Into a 20 mL screw-cap vial are weighed 48.8 mg of (1,5-cyclooctadiene)iridium chloride dimer (Strem, 0.145 mmol) and 56.6 mg of Diso (0.149 mmol, 1.03 equiv). To the vial is added 2 mL of dichloromethane. The vial is sealed with a Teflon-lined cap and shaken vigorously to dissolve the reagents, which react immediately to give a dark emerald green solution. The mixture is taken out of the drybox, and the solvent removed on a rotary evaporator. After the residue is slurried in 3 mL of acetonitrile, the green solid is suction filtered and the solid washed thoroughly with 1 mL of acetonitrile and air-dried 30 min to yield 81.2 mg of (Diso)Ir(cod)Cl (78%). $^1H$ NMR ($CD_2Cl_2$): $\delta$ 8.24 (d, 1.8 Hz, iminoxolene 3- or 5-H), 7.36 (t, 7.5 Hz, 1H, NAr 4-H), 7.17 (d, 7.5 Hz, 1H, NAr 3- or 5-H), 7.15 (d, 7.5 Hz, 1H, NAr 3- or 5-H), 7.12 (m, 1H, cod), 6.62 (d, 1.8 Hz, 1H, iminoxolene 3- or 5-H), 6.13 (m, 1H, cod), 5.06 (m, 1H, cod), 4.31 (m, 1H, cod), 4.01 (m, 1H cod), 3.36 (sept, 6.5 Hz, 1H, $CH(CH_3)_2$), 3.07 (m, 1H, cod), 2.53 (m, 2H, cod), 2.36 (m, 1H, cod), 2.26 (sept, 6.5 Hz, 1H, $CH(CH_3)_2$), 2.12 (m, 3H, cod), 1.55 (s, 9H, $^t$Bu), 1.08 (s, 9H, $^t$Bu), 1.20 (d, 6.5 Hz, 3H, $CH(CH_3)_2$), 1.09 (d, 6.5 Hz, 3H, $CH(CH_3)_2$), 0.93 (d, 6.5 Hz, 3H, $CH(CH_3)_2$), 0.87 (d, 6.5 Hz, 3H, $CH(CH_3)_2$). $^{13}C\{^1H\}$ NMR ($CD_2Cl_2$): 181.68 (CO), 165.55, 148.35, 147.23, 146.14, 139.74, 138.04, 129.09, 128.19, 125.14, 123.95, 117.28, 86.10 (cod alkene), 79.70 (cod alkene), 75.05 (cod alkene), 71.44 (cod alkene), 39.13, 36.38 ($C[CH_3]_3$), 35.89, 35.77 ($C[CH_3]_3$), 34.19, 30.76 ($C[CH_3]_3$), 29.53 ($C[CH_3]_3$), 28.28, 28.01 (2C), 26.10, 25.74, 24.84, 23.44. IR (ATR, $cm^{-1}$): 2958 (m), 2949 (m), 2971 (w), 2833 (w), 2867 (w), 2835 (w), 1528 (m), 1466 (m), 1450 (m), 1442 (m), 1392 (w), 1383 (m), 1360 (s), 1329 (m), 1305 (m), 1296 (m), 1263 (m), 1251 (s), 1237 (s), 1199 (m), 1159 (s), 1108 (m), 1096 (w), 1074 (w), 1051 (w), 1037 (w), 1027 (w), 1010 (m), 999 (m), 990 (w), 933 (w), 916 (m), 899 (s), 862 (s), 839 (m), 827 (m), 814 (m), 800 (s), 784 (s), 768 (s), 744 (s), 714 (m), 707 (m), 691 (w), 678 (m), 671 (w), 667 (w), 654 (m). UV−vis ($CH_2Cl_2$): $\lambda_{max}$ = 646 nm ($\varepsilon$ = 7400 L $mol^{-1}$ $cm^{-1}$), 460 nm (12700 L $mol^{-1}$ $cm^{-1}$). Anal. calcd for $C_{36}H_{55}ClIrNO$: C, 58.00; H, 7.44; N, 1.88. Found: C, 58.08; H, 7.11; N, 2.04.

**$(Diso)_2IrCl$.** Diso (450.7 mg, 0.594 mmol) and $[(coe)_2IrCl]_2$ (250.1 mg, 0.558 mmol Ir) are dissolved in 6 mL of benzene in a 20 mL scintillation vial. The vial is then capped and shaken until all the solids dissolve, and the resulting green solution is left to stand at room temperature for 3 d to allow precipitation of the product. The crystals are collected by filtration through a glass frit and washed with


https://doi.org/10.1021/acs.inorgchem.1c04005
Inorg. Chem. 2022, 61, 5547−5562

methanol (3 × 10 mL) and pentane (1 × 10 mL). The solid is dried *in vacuo* and then collected, yielding 507.3 mg (92%) of $(Diso)_2IrCl$. $^1H$ NMR ($CDCl_3$): $\delta$ 7.51 (d, 8 Hz, 2H, NAr 3- or 5-H), 7.41 (t, 8 Hz, 2H, NAr 4-H), 7.20 (d, 2 Hz, 2H, iminoxolene 3- or 5-H), 7.12 (d, 8 Hz, 2H, NAr 3- or 5-H), 6.59 (d, 2 Hz, 2H, iminoxolene 3- or 5-H), 3.09 (sept, 7 Hz, 2H, $CH(CH_3)_2$), 1.44 (d, 7 Hz, 6H, $CH(CH_3)_2$), 1.29 (s, 18H, $^t$Bu), 1.18 (s, 20H, $CH(CH_3)_2$, $^t$Bu), 1.06 (d, 7 Hz, 6H, $CH(CH_3)_2$), 0.81 (d, 7 Hz, 6H, $CH(CH_3)_2$), 0.16 (d, 7 Hz, 6H, $CH(CH_3)_2$). $^{13}C\{^1H\}$ NMR ($CDCl_3$): $\delta$ 179.02 (*C*O), 157.13, 146.95, 144.38, 141.74, 140.13, 138.44, 128.52, 124.58, 124.00, 123.43, 114.20, 35.40 ($C[CH_3]_3$), 34.80 ($C[CH_3]_3$), 31.26 ($C[CH_3]_3$), 29.93 ($C[CH_3]_3$), 29.00 ($CH[CH_3]_2$), 28.72 ($CH[CH_3]_2$), 25.35 ($CH[CH_3]_2$), 25.10 ($CH[CH_3]_2$), 24.90 ($CH[CH_3]_2$), 24.02 ($CH[CH_3]_2$). IR (nujol mull, $cm^{-1}$): 1587 (w), 1546 (w), 1530 (w), 1391 (m), 1378 (s), 1359 (s), 1329 (w), 1316 (w), 1284 (w), 1253 (s), 1232 (s), 1198 (s), 1179 (w), 1160 (s), 1106 (m), 1098 (m), 1057 (w), 1021 (m), 1001 (w), 936 (w), 918 (w), 863 (s), 779 (w), 741 (m), 652 (w), 606 (w). UV−vis ($CH_2Cl_2$): $\lambda_{max}$ = 710 ($\varepsilon$ = 9400 L $mol^{-1}$ $cm^{-1}$), 490 (sh, 8100 L $mol^{-1}$ $cm^{-1}$), 478 nm (8400 L $mol^{-1}cm^{-1}$). Anal. calcd for $C_{52}H_{74}ClIrN_2O_2$: C, 63.29; H, 7.56; N, 2.84. Found: C, 63.11; H, 8.00; N, 2.91.

**$(Diso)_2IrI$.** A mixture of $(Diso)_2IrCl$ (101.2 mg, 0.103 mmol) and sodium iodide (20.2 mg, 0.168 mmol) in 3 mL of acetone is stirred overnight under nitrogen. The resulting purple reaction mixture is exposed to the air and stripped down on the rotary evaporator. The solid is washed with 5 mL of water and 3 × 10 mL of MeOH and air-dried for 1 h to give 89.1 mg of $(Diso)_2IrI$ (80%). $^1H$ NMR ($CDCl_3$): $\delta$ 7.51 (d, 8 Hz, 2H, NAr 3- or 5-H), 7.40 (t, 8 Hz, 2H, NAr 4-H), 7.20 (d, 2 Hz, 2H, iminoxolene 3- or 5-H), 7.11 (d, 8 Hz, 2H, NAr 3- or 5-H), 6.47 (d, 2 Hz, 2H, Diso 3- or 5-H), 3.21 (sept, 7 Hz, 2H, $CH(CH_3)_2$), 1.48 (d, 7 Hz, 6H, $CH(CH_3)_2$), 1.38 (sept, 7 Hz, 2H, $CH(CH_3)_2$), 1.30 (s, 18H, $^t$Bu), 1.16 (s, 18H, $^t$Bu), 1.11 (d, 7 Hz, 6H, $CH(CH_3)_2$), 0.77 (d, 7 Hz, 6H, $CH(CH_3)_2$), 0.30 (d, 7 Hz, 6H, $CH(CH_3)_2$). $^{13}C\{^1H\}$ NMR ($CDCl_3$): $\delta$ 179.50 (*C*O), 156.08, 147.31, 142.87, 141.18, 138.89, 138.46, 128.34, 124.13, 123.44, 123.29, 114.60, 35.38 ($C[CH_3]_3$), 35.03 ($C[CH_3]_3$), 30.89 ($C[CH_3]_3$), 29.76 ($C[CH_3]_3$), 29.70 ($CH[CH_3]_2$), 29.14 ($CH[CH_3]_2$), 26.07 ($CH[CH_3]_2$), 25.54 ($CH[CH_3]_2$), 25.39 ($CH[CH_3]_2$), 23.79 ($CH[CH_3]_2$). IR (ATR, $cm^{-1}$): 3076 (w), 3062 (w), 2958 (s), 2926 (m), 2903 (w), 2865 (m), 1545 (w), 1538 (m), 1463 (m), 1457 (m), 1442 (m), 1392 (w), 1384 (w), 1359 (s), 1325 (m), 1314 (m), 1292 (w), 1284 (w), 1252 (s), 1228 (s), 1200 (s), 1178 (w), 1159 (s), 1109 (m), 1101 (m), 1055 (w), 1045 (w), 919 (m), 903 (w), 891 (m), 863 (m), 826 (m), 799 (m), 778 (m), 768 (w), 742 (s), 720 (w), 708 (w), 700 (w), 690 (w), 686 (w), 667 (m), 652 (m). UV−vis ($CH_2Cl_2$): $\lambda_{max}$ = 716 nm ($\varepsilon$ = 12900 L $mol^{-1}$ $cm^{-1}$), 555 nm (sh, 5600 L $mol^{-1}$ $cm^{-1}$), 507 nm (8000 L $mol^{-1}$ $cm^{-1}$). Anal. calcd for $C_{52}H_{74}IIrN_2O_2$: C, 57.92; H, 6.92, N, 2.60. Found: C, 57.55; H, 6.62; N, 2.61.

***trans*-$(Diso)_2IrCl_2$.** Into a 20 mL scintillation vial are weighed 89.3 mg of $(Diso)_2IrCl$ (0.090 mmol) and 30.3 mg of $PhICl_2$ (0.110 mmol). The reactants are dissolved in 5 mL of THF, and the purple solution is layered with 5 mL of $CH_3OH$ and allowed to stand for 3 d. The resulting crystals are collected by suction filtration and washed with 3 × 5 mL methanol. After drying *in vacuo*, the yield of *trans*-$(Diso)_2IrCl_2$ is 65.2 mg (70%). $^1H$ NMR ($CDCl_3$): $\delta$ 29.30 (v br), 14.81 (v br), 11.84 (br, 18H, $^t$Bu), 3.28 (br, 12H), 2.02 (br, 12H), 1.26 (br, 18H). $\mu_{eff}$ ($CDCl_3$): 1.932(6) $\mu_B$. IR ($cm^{-1}$): 3079 (w), 3062 (w), 2962 (m), 2953 (m), 2926 (m), 2904 (m), 2866 (m), 1588 (w), 1583 (w), 1513 (m), 1464 (m), 1395 (w), 1378 (w), 1345 (s), 1277 (s), 1243 (s), 1232 (s), 1193 (s), 1159 (s), 1089 (s), 1021 (s), 990 (s), 933 (w), 907 (m), 888 (m), 866 (m), 825 (w), 792 (m), 778 (m), 738 (s), 712 (m), 679 (w), 657 (w). UV−vis-NIR ($CCl_4$): 2029 nm ($\varepsilon$ = 10100 L $mol^{-1}$ $cm^{-1}$), 1685 nm (4900 L $mol^{-1}$ $cm^{-1}$), 1385 nm (6200 L $mol^{-1}$ $cm^{-1}$), 1148 nm (1400 L $mol^{-1}$ $cm^{-1}$), 788 nm (5800 $mol^{-1}$ $L^{-1}$ $cm^{-1}$), 756 nm (6000 L $mol^{-1}$ $cm^{-1}$), 676 nm (sh, 6400 L $mol^{-1}$ $cm^{-1}$), 618 nm (9600 L $mol^{-1}$ $cm^{-1}$), 492 nm (sh, 3600 L $mol^{-1}$ $cm^{-1}$), 432 nm (4700 L $mol^{-1}$ $cm^{-1}$), 413 nm (sh, 4400 L $mol^{-1}$ $cm^{-1}$), 364 nm (4200 L $mol^{-1}$ $cm^{-1}$), 313 nm (9100 L $mol^{-1}$ $cm^{-1}$). Anal. calcd for $C_{52}H_{74}Cl_2IrN_2O_2$: C, 61.10; H, 7.30; N, 2.74. Found: C, 60.93; H, 7.30; N, 2.86.

***cis*-$(Diso)_2IrCl_2$.** Diso (164.3 mg, 0.433 mmol) and $[(coe)_2IrCl]_2$ (93.5 mg, 0.208 mmol Ir) are added to a 50 mL Erlenmeyer flask containing a stir bar. The reactants are dissolved in approximately 2 mL of benzene, and the flask is brought out of the drybox and into a fume hood. In the hood, 4 mL of pentane and 4 mL of methanol are added, and the reaction mixture is allowed to stir, open to the air. After 3 days, 2 mL of $CH_3OH$ is added to replace any solvent that may have evaporated. After an additional 2 days, the solvents are removed on the rotary evaporator, and the purple solid is collected on a glass frit. Washing with 3 × 10 mL of $CH_3OH$ and air-drying for 30 min affords 66.4 mg (15%) of pure *cis*-$(Diso)_2IrCl_2$. At shorter reaction times, the compound is contaminated by a diamagnetic material, which can be removed by chromatography on silica gel, eluting with 2:1 $CH_2Cl_2$:hexanes and collecting the fraction with $R_f$ = 0.12. $^1H$ NMR ($CDCl_3$): $\delta$ 26.34 (br, 2H), 19.74 (br, 2H), 9.66 (br, 18H, $^t$Bu), 7.00 (br, 6H, $CH(CH_3)_2$), 5.45 (br, 12H), 4.27 (br, 2H), 1.55 (br, 2H), 1.15 (br, 6H, $CH(CH_3)_2$), 0.48 (br, 18H, $^t$Bu). $\mu_{eff}$ ($CDCl_3$): 1.599(2) $\mu_B$. IR ($cm^{-1}$): 3069 (w), 3056 (w), 2963 (m), 2951 (m), 2923 (m), 2864 (m), 1535 (w), 1513 (m), 1464 (m), 1440 (w), 1395 (w), 1380 (m), 1359 (m), 1348 (m), 1324 (m), 1304 (m), 1277 (w), 1248 (m), 1229 (s), 1199 (s), 1165 (s), 1090 (s), 1054 (w), 1026 (s), 985 (s), 951 (w), 933 (w), 916 (w), 906 (w), 886 (w), 876 (m), 865 (s), 825 (m), 798 (m), 768 (m), 737 (m), 706 (m), 676 (s). UV−vis-NIR ($CCl_4$): $\lambda_{max}$ = 2365 nm ($\varepsilon$ = 920 L $mol^{-1}$ $cm^{-1}$), 1803 nm (150 L $mol^{-1}$ $cm^{-1}$), 1413 nm (930 L $mol^{-1}$ $cm^{-1}$), 959 nm (1900 L $mol^{-1}$ $cm^{-1}$), 890 nm (sh, 1400 L $mol^{-1}$ $cm^{-1}$), 776 nm (sh, 1500 L $mol^{-1}$ $cm^{-1}$), 703 nm (5000 L $mol^{-1}$ $cm^{-1}$), 571 nm (3300 L $mol^{-1}$ $cm^{-1}$), 434 nm (2800 L $mol^{-1}$ $cm^{-1}$), 414 nm (sh, 2700 L $mol^{-1}$ $cm^{-1}$), 287 nm (7800 L $mol^{-1}$ $cm^{-1}$). Anal. calcd for $C_{52}H_{74}Cl_2IrN_2O_2$: C, 61.10; H, 7.30; N, 2.74. Found: C, 61.33; H, 7.26; N, 2.77.

**$(Diso)_2Ir$.** A mixture of 133.8 mg of $(Diso)_2IrCl$ (0.136 mmol) and 28.2 mg cobaltocene (Aldrich, 0.149 mmol) is dissolved in 5 mL of THF in a 20 mL scintillation vial. The vial is capped and shaken thoroughly and allowed to stand for 10 min. The resulting deep blue solution is filtered through a plug of cotton, then layered with 5 mL of $CH_3OH$ and placed in a −37 °C freezer. After 3 days, crystals are collected by suction filtration, washed with 3 × 5 mL of $CH_3OH$, and dried *in vacuo* to yield 91.7 mg $(Diso)_2Ir$ (71%). $^1H$ NMR (THF-$d_8$): $\delta$ 30.42 (br, 2H), 13.00 (br, 2H), 10.27 (br, 18H, $^t$Bu), 2.27 (br, 2H), 1.58 (br), − 1.34 (br), − 2.29 (br, 18H, $^t$Bu), − 20.51 (br). $\mu_{eff}$ (THF-$d_8$): 1.59(2) $\mu_B$. IR (nujol mull, $cm^{-1}$): 1581 (m), 1545 (m), 1377 (s), 1359 (s), 1329 (s), 1289 (s), 1257 (s) 1228 (w), 1219 (w), 1199 (w), 1177 (m), 1151 (s), 1109 (w), 1100 (w), 1073 (w), 1056 (w), 1041 (w), 1026 (w), 997 (w), 937 (w), 923 (w), 863 (m), 828 (m), 801 (m), 770 (m), 739 (s), 696 (w), 669 (w), 652 (w). UV−vis ($CH_2Cl_2$): $\lambda_{max}$ = 757 nm (sh, $\varepsilon$ = 5400 L $mol^{-1}$ $cm^{-1}$), 697 nm (sh, 9000 L $mol^{-1}$ $cm^{-1}$), 634 nm (25900 L $mol^{-1}$ $cm^{-1}$). Anal. calcd for $C_{52}H_{74}IrN_2O_2$: C, 65.65; H, 7.84, N, 2.94. Found: C, 65.28; H, 7.88; N, 2.92.

**Cyclic Voltammetry.** Cyclic voltammograms were performed at a scan rate of 60 $mV{\cdot}s^{-1}$ using a Metrohm Autolab PGSTAT128N potentiostat, with glassy carbon working and counter electrodes and a silver/silver chloride pseudoreference electrode. The electrodes were connected to the potentiostat through electrical conduits in the drybox wall. Samples were 1 mM in analyte dissolved in $CH_2Cl_2$ with 0.1 M $Bu_4NPF_6$ as the electrolyte. Potentials were referenced to ferrocene/ferrocenium at 0 V.[48] The reference potential of $(Diso)_2IrI$ was established by spiking the test solution with a small amount of ferrocene, while all other compounds were referenced by spiking with decamethylferrocene ($E^\circ$ = −0.565 V vs $Cp_2Fe^+/Cp_2Fe$).[49]

**X-ray Crystallography.** Crystals of $(Diso)Ir(cod)Cl{\cdot}CH_3CN$ were deposited from a solution of the complex in acetonitrile. Crystals of $(Diso)_2IrCl{\cdot}3C_6H_6$ were grown by liquid diffusion of pentane into a benzene solution of the complex, while crystals of $(Diso)_2IrI{\cdot}C_3H_6O$ deposited on slow evaporation of an acetone solution of the complex. Crystals of *cis*- and *trans*-$(Diso)_2IrCl_2$ were grown by liquid diffusion of $CH_3OH$ into $CH_2Cl_2$ (with the *trans*


https://doi.org/10.1021/acs.inorgchem.1c04005
Inorg. Chem. 2022, 61, 5547−5562

compound being generated *in situ* from $(Diso)_2IrCl$ and $PhICl_2$). Crystals of $(Diso)_2Ir$ were deposited from a solution in THF after layering with $CH_3OH$ and storage at −37 °C.

Crystals were placed in inert oil before being transferred to the cold $N_2$ stream of either a Bruker Apex II or a Bruker Kappa X8-Apex-II CCD diffractometer. The data were reduced, correcting for absorption, using the program SADABS. The structures were all solved either from a Patterson map ((Diso)Ir(cod)Cl·0.5 $CH_3CN$, $(Diso)_2IrCl·3C_6H_6$) or by direct methods (all others). All non-hydrogen atoms were located on difference Fourier maps, and all were refined anisotropically except for C41 in $(Diso)_2IrI·C_3H_6O$, which did not refine successfully and was constrained to share the thermal parameters of the other *ipso* carbon in the molecule, C21. $(Diso)_2IrCl·3C_6H_6$ crystallized in the chiral space group $P2_12_12$, but was refined as a racemic twin. In (Diso)Ir(cod)Cl·0.5 $CH_3CN$, the lattice acetonitrile was found to be disordered about the inversion center and was modeled by refining it at half occupancy.

Hydrogen atoms were found on difference maps and refined isotropically, except in the structure of $(Diso)_2IrI·C_3H_6O$, the lattice $CH_3CN$ in (Diso)Ir(cod)Cl·0.5 $CH_3CN$, and the *tert*-butyl group centered at C18 and the lattice benzene in general position in $(Diso)_2IrCl·3C_6H_6$. In these cases, hydrogen atoms were placed in calculated positions with their thermal parameters tied to the isotropic thermal parameters of the atoms they are bonded (1.5× for methyl, 1.2× for all others). Calculations used SHELXTL (Bruker AXS),[50] with scattering factors and anomalous dispersion terms taken from literature.[51] Further details are in Table 1.

**EPR Measurements.** Spectra were acquired on frozen solutions of the compounds at 10 K. The samples were made up in the drybox in 4 mm quartz tubes sealed with Teflon-lined screwcaps. Samples were frozen in liquid $N_2$ before they were inserted into the EPR cavity. The samples were then cooled to 10 K and were allowed to equilibrate for 15 min before spectra were taken. All measurements were conducted on a Bruker EMX X-band (9.624 GHz) EPR spectrometer using a power of 2.179 mW and a modulation amplitude of 4.00 G.

**Computational Methods.** Geometry optimizations were performed on CpIr(ap), (ap)Ir(cod)Cl, $(ap)_2IrCl$, $(ap)_2IrI$, $(ap)_2Ir$, and *cis*- and *trans*-$(ap)_2IrCl_2$ (ap = *o*-$C_6H_4(NPh)O$) using density functional theory (B3LYP, SDD basis set for Ir and I, 6-31G* basis set for all other atoms), using the Gaussian 16 suite of programs.[52] X-ray structures were used as initial geometries, with all *tert*-butyl and methyl groups replaced by hydrogen. The optimized geometries were confirmed as minima by calculation of vibrational frequencies. Plots of calculated Kohn−Sham orbitals were generated using Gaussview (v. 6.0.16) with an isovalue of 0.04.

## ■ ASSOCIATED CONTENT

### Supporting Information

The Supporting Information is available free of charge at https://pubs.acs.org/doi/10.1021/acs.inorgchem.1c04005.

> Characterization of *cis*-$(Diso)_2Ir(\mu\text{-}Cl)_2Ir(coe)_2$, thermal ellipsoid plot of $(Diso)_2IrI$, cyclic voltammograms, NMR spectra, optical spectrum of (Diso)Ir(cod)Cl, Cartesian coordinates and calculated energies and MOS values by DFT (PDF)

### Accession Codes

CCDC 2095661−2095667 contain the supplementary crystallographic data for this paper. These data can be obtained free of charge via www.ccdc.cam.ac.uk/data_request/cif, or by emailing data_request@ccdc.cam.ac.uk, or by contacting The Cambridge Crystallographic Data Centre, 12 Union Road, Cambridge CB2 1EZ, UK; fax: +44 1223 336033.

## ■ AUTHOR INFORMATION


### Corresponding Author

**Seth N. Brown** − *Department of Chemistry and Biochemistry, University of Notre Dame, Notre Dame, Indiana 46556-5670, United States;* orcid.org/0000-0001-8414-2396; Email: Seth.N.Brown.114@nd.edu

### Author

**Thomas H. Do** − *Department of Chemistry and Biochemistry, University of Notre Dame, Notre Dame, Indiana 46556-5670, United States*

Complete contact information is available at: https://pubs.acs.org/10.1021/acs.inorgchem.1c04005


### Notes

The authors declare no competing financial interest.

## ■ ACKNOWLEDGMENTS

This work was supported by the US National Science Foundation (grants CHE-1465104 and CHE-1955933). We thank Dr. Allen G. Oliver for his assistance with X-ray crystallography and Kahargyan Nugraha and Maximilian Meißner for their assistance with the spectroscopic characterization of $(Diso)_2Ir$. T.H.D. acknowledges support via an Arthur J. Schmitt Fellowship.

## ■ REFERENCES


(1) Poddel'sky, A. I.; Cherkasov, V. K.; Abakumov, G. A. Transition metal complexes with bulky 4,6-di-*tert*-butyl-*N*-aryl(alkyl)-o-iminobenzoquinonato ligands: Structure, EPR and magnetism. *Coord. Chem. Rev.* **2009**, *253*, 291−324.

(2) Pierpont, C. G. Studies on charge distribution and valence tautomerism in transition metal complexes of catecholate and semiquinonate ligands. *Coord. Chem. Rev.* **2001**, *216−217*, 99−125.

(3) Gordon, D. J.; Fenske, R. F. Theoretical Study of *o*-Quinone Complexes of Chromium and Vanadium. *Inorg. Chem.* **1982**, *21*, 2907−2915.

(4) Marshall-Roth, T.; Brown, S. N. Redox activity and $\pi$ bonding in a tripodal seven-coordinate molybdenum(VI) tris(amidophenolate). *Dalton Trans.* **2015**, *44*, 677−685.

(5) Do, T. H.; Brown, S. N. Synthesis, dynamics and redox properties of eight-coordinate zirconium catecholate complexes. *Dalton Trans.* **2020**, *49*, 11648−11656.

(6) Blackmore, K. J.; Ziller, J. W.; Heyduk, A. F. Oxidative Addition" to a Zirconium(IV) Redox-Active Ligand Complex. *Inorg. Chem.* **2005**, *44*, 5559−5561.

(7) Heyduk, A. F.; Zarkesh, R. A.; Nguyen, A. I. Designing Catalysts for Nitrene Transfer Using Early Transition Metals and Redox-Active Ligands. *Inorg. Chem.* **2011**, *50*, 9849−9863.

(8) Hananouchi, S.; Krull, B. T.; Ziller, J. W.; Furche, F.; Heyduk, A. F. Metal effects on ligand non-innocence in Group 5 complexes of the redox-active [ONO] pincer ligand. *Dalton Trans.* **2014**, *43*, 17991−18000.

(9) Sun, X.; Chun, H.; Hildenbrand, K.; Bothe, E.; Weyhermüller, T.; Neese, F.; Wieghardt, K. *o*-Iminobenzosemiquinonato(1−) and *o*-Amidophenolato(2−) Complexes of Palladium(II) and Platinum(II): A Combined Experimental and Density Functional Theoretical Study. *Inorg. Chem.* **2002**, *41*, 4295−4303.

(10) Kokatam, S.; Weyhermüller, T.; Bothe, E.; Chaudhuri, P.; Wieghardt, K. Structural Characterization of Four Members of the Electron-Transfer Series $[Pd^{II}(L)_2]^n$ (L = *o*-Iminophenolate Derivative; $n$ = 2−, 1−, 0, 1+, 2+). Ligand Mixed Valency in the Monocation and Monoanion with $S$ = 1/2 Ground States. *Inorg. Chem.* **2005**, *44*, 3709−3717.

(11) Conner, K. M.; Perugini, A. L.; Malabute, M.; Brown, S. N. Group 10 Bis(iminosemiquinone) Complexes: Measurement of

Singlet−Triplet Gaps and Analysis of the Effects of Metal and Geometry on Electronic Structure. *Inorg. Chem.* **2018**, *57*, 3272−3286.
(12) Erickson, A. N.; Brown, S. N. Molybdenum(VI) tris(amidophenoxide) complexes. *Dalton Trans.* **2018**, *47*, 15583−15595.
(13) Gianino, J.; Brown, S. N. Highly covalent metal−ligand $\pi$ bonding in chelated bis- and tris(iminoxolene) complexes of osmium and ruthenium. *Dalton Trans.* **2020**, *49*, 7015−7027.
(14) Gianino, J.; Erickson, A. N.; Markovitz, S. J.; Brown, S. N. High-valent osmium iminoxolene complexes. *Dalton Trans.* **2020**, *49*, 8504−8515.
(15) Ringenberg, M. R.; Kokatam, S. L.; Heiden, Z. M.; Rauchfuss, T. B. Redox-switched oxidation of dihydrogen using a non-innocent ligand. *J. Am. Chem. Soc.* **2008**, *130*, 788−789.
(16) Ringenberg, M. R.; Nilges, M. J.; Rauchfuss, T. B.; Wilson, S. R. Oxidation of Dihydrogen by Iridium Complexes of Redox-Active Ligands. *Organometallics.* **2010**, *29*, 1956−1965.
(17) Hübner, R.; Weber, S.; Strobel, S.; Sarkar, B.; Záliš, S.; Kaim, W. Reversible Intramolecular Single-Electron Oxidative Addition Involving a Hemilabile Noninnocent Ligand. *Organometallics* **2011**, *30*, 1414−1418.
(18) Abakumov, G. A.; Druzhkov, N. O.; Kurskii, Y. A.; Shavyrin, A. S. NMR study of products of thermal transformation of substituted *N*-aryl-*o*-quinoneimines. *Russ. Chem. Bull.* **2003**, *52*, 712−717.
(19) Smolyaninov, I. V.; Letichevskaya, N. N.; Kulakov, A. V.; Aref'ev, Y. B.; Pashchenko, K. P.; Berberova, N. T. Study of the Mechanism of Redox Transformations of Sterically Hindered *N*-Aryl-*o*-iminoquinones. *Russ. J. Electrochem.* **2007**, *43*, 1187−1199.
(20) Brown, S. N. Metrical Oxidation States of 2-Amidophenoxide and Catecholate Ligands: Structural Signatures of Metal−Ligand $\pi$ Bonding in Potentially Noninnocent Ligands. *Inorg. Chem.* **2012**, *51*, 1251−1260.
(21) Addison, A. W.; Rao, T. N.; Reedijk, J.; van Rijn, J.; Verschoor, G. C. Synthesis, Structure, and Spectroscopic Properties of Copper(II) Compounds containing Nitrogen-Sulphur Donor Ligands; the Crystal and Molecular Structure of Aqua[1,7-bis(*N*-methylbenzimidazol-2′-yl)-2,6-dithiaheptane]copper(II) Perchlorate. *J. Chem. Soc., Dalton Trans.* **1984**, 1349−1356.
(22) Kaim, W.; Sieger, M.; Greulich, S.; Sarkar, B.; Fiedler, J.; Záliš, S. The 1,4-diazabutadiene/1,2-enediamido non-innocent ligand system in the formation of iridaheteroaromatic compounds: Spectroelectrochemistry and electronic structure. *J. Organomet. Chem.* **2010**, *695*, 1052−1058.
(23) Hartl, F.; Vlček, A.; deLearie, L. A.; Pierpont, C. G. Oxidative Substitution of $Mn(CO)_5^-$ by 3,5-Di-*tert*-butyl-1,2-benzoquinone. Synthesis and Characterization of the Unsaturated $Mn(CO)_3(DBCat)^-$ Anion. *Inorg. Chem.* **1990**, *29*, 1073−1078.
(24) Green, M. L. H. A new approach to the formal classification of covalent compounds of the elements. *J. Organomet. Chem.* **1995**, *500*, 127−148.
(25) (a) Mason, R.; Thomas, K. M.; Empsall, H. D.; Fletcher, S. R.; Heys, P. N.; Hyde, E. M.; Jones, C. E.; Shaw, B. L. Synthesis and Structural Characteristics of Planar Iridium(II) Complexes. *J. Chem. Soc., Chem. Commun.* **1974**, 612−614. (b) Danopoulos, A. A.; Wilkinson, G.; Hussain-Bates, B.; Hursthouse, M. B. Bis(diethyl sulfide)bis(2,4,6-trimethylphenyl)iridium(II) and Related Compounds. *J. Chem. Soc., Dalton Trans.* **1992**, 3165−3170. (c) García, M. P.; Jiménez, M. V.; Oro, L. A.; Lahoz, F. J.; Alonso, P. J. A Paramagnetic, Mononuclear Organometallic Iridium(II) Complex: $[Ir(C_6Cl_5)_2(cod)]$. *Angew. Chem., Int. Ed.* **1992**, *31*, 1527−1529. (d) García, M. P.; Jiménez, M. V.; Oro, L. A.; Lahoz, F. J.; Tiripicchio, M. C.; Tiripicchio, A. A Homoleptic Mononuclear Iridium(II) Organometallic Complex: Synthesis and X-ray Structure of $[Ir(C_6Cl_5)_4]^{2-}$. *Organometallics* **1993**, *12*, 4660−4663. (e) Zhai, H.; Bunn, A.; Wayland, B. Formation and ethene substrate reactions of iridium(II) porphyrin metal-centered d$\pi$ radicals. *Chem. Commun.* **2001**, 1294−1295.
(26) (a) Ionkin, A. S.; Marshall, W. J. Rare Organometallic Complex of Divalent, Four-Coordinate Iridium: Synthesis, Structural Characterization, and First Insights into Reactivity. *Organometallics* **2004**, *23*, 6031−6041. (b) Meiners, J.; Scheibel, M. G.; Lemée-Cailleau, M.-H.; Mason, S. A.; Boeddinghaus, M. B.; Fässler, T. F.; Herdtweck, E.; Khusniyarov, M. M.; Schneider, S. Square-Planar Iridium(II) and Iridium(III) Amido Complexes Stabilized by a PNP Pincer Ligand. *Angew. Chem., Int. Ed.* **2011**, *50*, 8184−8187.
(27) (a) Kubota, M.; Chan, M. K.; Boyd, D. C.; Mann, K. R. Thermal and photolytic reactions of nitrosyl-carbonyl complexes of rhodium and iridium with triphenylphosphine. *Inorg. Chem.* **1987**, *26*, 3261−3264. (b) de Bruin, B.; Peters, T. P. J.; Thewissen, S.; Blok, A. N. J.; Wilting, J. B. M.; de Gelder, R.; Smits, J. M. M.; Gal, A. W. Dioxygen Activation by a Mononuclear $Ir^{II}$ − Ethene Complex. *Angew. Chem., Int. Ed.* **2002**, *41*, 2135−2138. (c) Takaoka, A.; Peters, J. C. A Homologous Series of Cobalt, Rhodium, and Iridium Metalloradicals. *Inorg. Chem.* **2012**, *51*, 16−18. (d) Fuchigami, K.; Rath, N. P.; Mirica, L. M. Mononuclear Rhodium(II) and Iridium(II) Complexes Supported by Tetradentate Pyridinophane Ligands. *Inorg. Chem.* **2017**, *56*, 9404−9408.
(28) Herebian, D.; Wieghardt, K. E.; Neese, F. Analysis and Interpretation of Metal-Radical Coupling in a Series of Square Planar Nickel Complexes: Correlated Ab Initio and Density Functional Investigation of $[Ni(L^{ISQ})_2]$ ($L^{ISQ}$ = 3,5-di-*tert*-butyl-*o*-diiminobenzosemiquinonate(1−)). *J. Am. Chem. Soc.* **2003**, *125*, 10997−11005.
(29) Cipressi, J.; Brown, S. N. Octahedral to trigonal prismatic distortion driven by subjacent orbital $\pi$ antibonding interactions and modulated by ligand redox noninnocence. *Chem. Commun.* **2014**, *50*, 7956−7959.
(30) Bill, E.; Bothe, E.; Chaudhuri, P.; Chlopek, K.; Herebian, D.; Kokatam, S.; Ray, K.; Weyhermüller, T.; Neese, F.; Wieghardt, K. Molecular and Electronic Structure of Four- and Five-Coordinate Cobalt Complexes Containing Two *o*-Phenylenediamine- or Two *o*-Aminophenol-Type Ligands at Various Oxidation Levels: An Experimental, Density Functional, and Correlated ab initio Study. *Chem.—Eur. J.* **2005**, *11*, 204−224.
(31) Erickson, A. N.; Gianino, J.; Markovitz, S. J.; Brown, S. N. Amphiphilicity in Oxygen Atom Transfer Reactions of Oxobis(iminoxolene)osmium Complexes. *Inorg. Chem.* **2021**, *60*, 4004−4014.
(32) Cooper, A. C.; Streib, W. E.; Eisenstein, O.; Caulton, K. G. *tert*-Butyl is Superior to Phenyl as an Agostic Donor to 14-Electron Ir(III). *J. Am. Chem. Soc.* **1997**, *119*, 9069−9070.
(33) Jacobi, B. G.; Laitar, D. S.; Pu, L.; Wargocki, M. F.; DiPasquale, A. G.; Fortner, K. C.; Schuck, S. M.; Brown, S. N. Stoichiometric and Catalytic Oxygen Activation by Trimesityliridium(III). *Inorg. Chem.* **2002**, *41*, 4815−4823.
(34) (a) Smith, A. L.; Clapp, L. A.; Hardcastle, K. I.; Soper, J. D. Redox-active ligand-mediated Co−Cl bond-forming reactions at reducing square planar cobalt(III) centers. *Polyhedron* **2010**, *29*, 164−169. (b) Piskunov, A. V.; Pashanova, K. I.; Bogomyakov, A. S.; Smolyaninov, I. V.; Starikov, A. G.; Fukin, G. K. Cobalt complexes with hemilabile *o*-iminobenzoquinonate ligands: a novel example of redox-induced electron transfer. *Dalton Trans.* **2018**, *47*, 15049−15060. (c) Salojärvi, E.; Peuronen, A.; Huhtinen, H.; Vlasenko, L. S.; Halme, J.; Mäkinen, P.; Lastusaari, M.; Lehtonen, A. NIR-absorbing transition metal complexes with redox-active ligands. *Inorg. Chem. Commun.* **2020**, *112*, 107711.
(35) (a) Poddel'sky, A. I.; Cherkasov, V. K.; Fukin, G. K.; Bubnov, M. P.; Abakumova, L. G.; Abakumov, G. A. New four- and five-coordinated complexes of cobalt with sterically hindered *o*-iminobenzoquinone ligands: synthesis and structure. *Inorg. Chim. Acta* **2004**, *357*, 3632−3640. (b) Piskunov, A. V.; Pashanova, K. I.; Ershova, I. V.; Bogomyakov, A. S.; Starikov, A. G.; Cherkasov, A. V. Synthesis of four-, five-, and six-coordinate cobalt(III) bis-*o*-iminobenzosemiquinone complexes. *Russ. Chem. Bull.* **2019**, *68*, 757−769.
(36) Paul, G. C.; Ghorai, S.; Mukherjee, C. Monoradical-containing four-coordinate Co(III) complexes: homolytic S−S and Se−Se bond


https://doi.org/10.1021/acs.inorgchem.1c04005
*Inorg. Chem.* 2022, 61, 5547−5562

cleavage and catalytic isocyanate to urea conversion under sunlight. *Chem. Commun.* **2017**, *53*, 8022−8025.
(37) (a) Herebian, D.; Ghosh, P.; Chun, H.; Bothe, E.; Weyhermüller, T.; Wieghardt, K. Cobalt(II)/(III) Complexes Containing *o*-Iminothiobenzosemiquinonato(1−) and *o*-Iminobenzosemiquinonato(1−) π-Radical Ligands. *Eur. J. Inorg. Chem.* **2002**, *2002*, 1957−1967. (b) Maity, S.; Kundu, S.; Bera, S.; Weyhermüller, T.; Ghosh, P. Mixed-Valence *o*-Iminobenzoquinone and *o*-Iminobenzosemiquinonate Anion Radical Complexes of Cobalt: Valence Tautomerism. *Eur. J. Inorg. Chem.* **2016**, *2016*, 3680−3690.
(38) Smith, A. L.; Hardcastle, K. I.; Soper, J. D. Redox-Active Ligand-Mediated Oxidative Addition and Reductive Elimination at Square Planar Cobalt(III): Multielectron Reactions for Cross-Coupling. *J. Am. Chem. Soc.* **2010**, *132*, 14358−14360.
(39) (a) Verani, C. N.; Gallert, S.; Bill, E.; Weyhermüller, T.; Wieghardt, K.; Chaudhuri, P. [Tris(*o*-iminosemiquinone)cobalt-(III)]—a radical complex with an $S_t = {}^3/_2$ ground state. *Chem. Commun.* **1999**, 1747−1748. (b) Mukherjee, S.; Rentschler, E.; Weyhermüller, T.; Wieghardt, K.; Chaudhuri, P. A unique series of dinuclear transition metal−polyradical complexes with a *m*-phenylenediamine spacer and their catalytic reactivity. *Chem. Commun.* **2003**, 1828−1829. (c) Dei, A.; Gatteschi, D.; Sangregorio, C.; Sorace, L.; Vaz, M. G. F. Bonding Coordination Requirements Induce Antiferromagnetic Coupling between *m*-Phenylene Bridged *o*-Iminosemiquinonato Diradicals. *Inorg. Chem.* **2003**, *42*, 1701−1706. (d) Chaudhuri, P.; Wagner, R.; Pieper, U.; Biswas, B.; Weyhermüller, T. Effect of the substituents on the spin coupling between iminosemiquinone π-radicals mediated by diamagnetic metal ions: l.s. Co(III) *vs* Ga(III). *Dalton Trans.* **2008**, 1286−1288.
(40) Chirik, P. J.; Wieghardt, K. Radical Ligands Confer Nobility on Base-Metal Catalysts. *Science* **2010**, *327*, 794−795.
(41) Ershova, I. V.; Smolyaninov, I. V.; Bogomyakov, A. S.; Fedin, M. V.; Starikov, A. G.; Cherkasov, A. V.; Fukin, G. K.; Piskunov, A. V. Tetrahedral nickel(II) and cobalt(II) bis-*o*-iminobenzosemiquinonates. *Dalton Trans.* **2019**, *48*, 10723−10732.
(42) (a) Munhá, R. F.; Zarkesh, R. A.; Heyduk, A. F. Group transfer reactions of $d^0$ transition metal complexes: redox-active ligands provide a mechanism for expanded reactivity. *Dalton Trans.* **2013**, *42*, 3751−3766. (b) Broere, D. L. J.; Plessius, R.; van der Vlugt, J. I. New avenues for ligand-mediated processes − expanding metal reactivity by the use of redox-active catechol, *o*-aminophenol and *o*-phenylenediamine ligands. *Chem. Soc. Rev.* **2015**, *44*, 6886−6915.
(43) Wolczanski, P. T. Flipping the Oxidation State Formalism: Charge Distribution in Organometallic Complexes as Reported by Carbon Monoxide. *Organometallics* **2017**, *36*, 622−631.
(44) Herde, J. L.; Lambert, J. C.; Senoff, C. V.; Cushing, M. A. Cyclooctene and 1,5-Cyclooctadiene Complexes of Iridium(I). *Inorg. Synth.* **2007**, *15*, 18−20.
(45) Tao, J.; Tran, R.; Murphy, G. K. Dihaloiodoarenes: α,α-Dihalogenation of Phenylacetate Derivatives. *J. Am. Chem. Soc.* **2013**, *135*, 16312−16315.
(46) (a) Sur, S. K. Measurement of Magnetic Susceptibility and Magnetic Moment of Paramagnetic Molecules in Solution by High-Field Fourier Transform NMR Spectroscopy. *J. Magn. Reson.* **1989**, *82*, 169−173. (b) Schubert, E. M. Utilizing the Evans Method with a Superconducting NMR Spectrometer in the Undergraduate Laboratory. *J. Chem. Educ.* **1992**, *69*, 62.
(47) Ranis, L. G.; Werellapatha, K.; Pietrini, N. J.; Bunker, B. A.; Brown, S. N. Metal and Ligand Effects on Bonding in Group 6 Complexes of Redox-Active Amidodiphenoxides. *Inorg. Chem.* **2014**, *53*, 10203−10216.
(48) Connelly, N. G.; Geiger, W. E. Chemical Redox Agents for Organometallic Chemistry. *Chem. Rev.* **1996**, *96*, 877−910.
(49) Lionetti, D.; Medvecz, A. J.; Ugrinova, V.; Quiroz-Guzman, M.; Noll, B. C.; Brown, S. N. Redox-Active Tripodal Aminetris(aryloxide) Complexes of Titanium(IV). *Inorg. Chem.* **2010**, *49*, 4687−4697.
(50) Sheldrick, G. M. A short history of SHELX. *Acta Crystallogr., Sect. A: Found. Crystallogr.* **2008**, *64*, 112−122.
(51) Wilson, A. J. C.; Geist, V. *International Tables for Crystallography, Vol. C: Mathematical, Physical and Chemical Tables*; Kluwer Academic Publishers: Dordrecht/Boston/London, 1992.
(52) Frisch, M. J.; Trucks, G. W.; Schlegel, H. B.; Scuseria, G. E.; Robb, M. A.; Cheeseman, J. R.; Scalmani, G.; Barone, V.; Petersson, G. A.; Nakatsuji, H.; Li, X.; Caricato, M.; Marenich, A. V.; Bloino, J.; Janesko, B. G.; Gomperts, R.; Mennucci, B.; Hratchian, H. P.; Ortiz, J. V.; Izmaylov, A. F.; Sonnenberg, J. L.; Williams-Young, D.; Ding, F.; Lipparini, F.; Egidi, F.; Goings, J.; Peng, B.; Petrone, A.; Henderson, T.; Ranasinghe, D.; Zakrzewski, V. G.; Gao, J.; Rega, N.; Zheng, G.; Liang, W.; Hada, M.; Ehara, M.; Toyota, K.; Fukuda, R.; Hasegawa, J.; Ishida, M.; Nakajima, T.; Honda, Y.; Kitao, O.; Nakai, H.; Vreven, T.; Throssell, K.; Montgomery, J. A., Jr.; Peralta, J. E.; Ogliaro, F.; Bearpark, M. J.; Heyd, J. J.; Brothers, E. N.; Kudin, K. N.; Staroverov, V. N.; Keith, T. A.; Kobayashi, R.; Normand, J.; Raghavachari, K.; Rendell, A. P.; Burant, J. C.; Iyengar, S. S.; Tomasi, J.; Cossi, M.; Millam, J. M.; Klene, M.; Adamo, C.; Cammi, R.; Ochterski, J. W.; Martin, R. L.; Morokuma, K.; Farkas, O.; Foresman, J. B.; Fox, D. J. *Gaussian 16*, Revision C.01; Gaussian, Inc.: Wallingford, CT, 2016.




https://doi.org/10.1021/acs.inorgchem.1c04005
*Inorg. Chem.* 2022, 61, 5547−5562